Universality of the Lyapunov regime for the Loschmidt echo

Fernando M. Cucchietti,[1,2] Horacio M. Pastawski,[2] and Rodolfo A. Jalabert[3]
[1]*Theoretical Division, MS B213, Los Alamos National Laboratory, Los Alamos, New Mexico 87545, USA*
[2]*Facultad de Matemática, Astronomía y Física, Universidad Nacional de Córdoba, Ciudad Universitaria, 5000 Córdoba, Argentina*
[3]*Institut de Physique et Chimie des Matériaux de Strasbourg, UMR 7504, CNRS-ULP, 23 rue du Loess, Boîte Postale 43, 67034 Strasbourg Cedex 2, France*

(Received 31 July 2003; revised manuscript received 1 December 2003; published 22 July 2004)

The Loschmidt echo (LE) is a magnitude that measures the sensitivity of quantum dynamics to perturbations in the Hamiltonian. For a certain regime of the parameters, the LE decays exponentially with a rate given by the Lyapunov exponent of the underlying classically chaotic system. We develop a semiclassical theory, supported by numerical results in a Lorentz gas model, which allows us to establish and characterize the universality of this Lyapunov regime. In particular, the universality is evidenced by the semiclassical limit of the de Broglie wavelength going to zero, the behavior for times longer than Ehrenfest time, the insensitivity with respect to the form of the perturbation, and the behavior of individual (nonaveraged) initial conditions. Finally, by elaborating a semiclassical approximation to the Wigner function, we are able to distinguish between classical and quantum origin for the different terms of the LE. This approach renders an understanding for the persistence of the Lyapunov regime after the Ehrenfest time, as well as a reinterpretation of our results in terms of the quantum-classical transition.

DOI: 10.1103/PhysRevB.70.035311 PACS number(s): 03.65.Sq, 03.65.Yz, 05.45.Mt, 03.67.−a

I. INTRODUCTION

Controlling the phase in the evolution of a quantum system is a fundamental problem that is becoming increasingly relevant in many areas of physics. In relatively simple systems, such as a quantum dot in an Aharanov-Bohm ring,[1] the phase can even be measured by transport experiments. The development of the quantum information field requires the control of the phase of increasingly complex systems.[2] Such a control is hindered by interactions with the environment in a way which is not completely understood at present.

Nuclear magnetic resonance provides a privileged framework to test our ideas on the evolution and degradation of the quantum phase. The phenomenon of spin echo, through the reversal of the time evolution, allows us to study how an individual spin, in an ensemble, loses its phase memory.[3] The randomization of its phase appears as a consequence of the interaction with other spins that act as an environment. Recently, it has become possible to test the phase of the collective many-spin state through the experiments of magic[4] and polarization[5] echoes. In these cases an initial polarization ''diffuses'' away as consequence of the spin-spin interactions in the effective Hamiltonian $\mathcal{H}$. The whole many-body dynamics can be reversed by the sudden transformation $\mathcal{H}\rightarrow -\mathcal{H}$. However, there is a failure to recover the initial polarization state which increases with the time elapsed before the reversal. Such a failure is a consequence of the fluctuations of the phase of the complex quantum state[6] and constitutes a measure of the entropy growth.[7]

Surprisingly, the rate of phase information loss appears as an intrinsic property of the system, quite insensitive to how small the coupling to the external degrees of freedom is, or to the precision of the reversal.[8] This may be interpreted as analogous to the residual resistivity of impure metals. When the direct coupling to the thermal bath is decreased by lowering the temperature, the resistivity becomes controlled by the reversible elastic scattering with impurities.[9,10] The common feature of both intrinsic behaviors is the complexity of the dynamics that justifies the *stosszahlansatz* or molecular chaos hypothesis.

However, such a hypothesis does not seem to be compatible with our basic knowledge of quantum dynamics. Unlike classical mechanics, quantum dynamics does not exhibit hypersensitivity to initial conditions.[11,12] That is why the field known as quantum chaos deals mainly with the quantum stationary properties of systems whose underlying classical dynamics is chaotic. Among these properties, the ones more frequently studied are the level statistics,[13] wave-function scarring,[14] and parametric correlations.[15] A notable exception among these studies was that of Peres,[16] who realized that, for long times, classically chaotic and integrable systems behave differently under imperfect time reversal. It is through the experimental findings above cited that the study of time evolution of classically chaotic systems has gained a privileged place in nowadays research.

A simplified version of the echoes experimentally studied is the so-called Loschmidt echo (LE)

$$M(t)=|m(t)|^2=|\langle\psi_0|e^{i(\mathcal{H}_0+\Sigma)t/\hbar}e^{-i\mathcal{H}_0 t/\hbar}|\psi_0\rangle|^2, \quad (1.1)$$

where $|\psi_0\rangle$ is an arbitrary initial state that evolves forward in time under the system Hamiltonian $\mathcal{H}_0$ for a time t, and then backwards under a slightly perturbed Hamiltonian $\mathcal{H}_0+\Sigma$ between t and $2t$. The amplitude $m(t)$ of the LE also represents the overlap between the two slightly different evolutions of the same initial state and $M(t)$ quantifies the departure from the perfect overlap. Because of this important property, within the field of quantum information the LE is referred to as *fidelity*.[17] Alternatively, $M(t)$ can also be written as the trace of the product of two pure-state density matrices ρ or Wigner functions W evolving with different Hamiltonians,

$$M(t)=\mathrm{tr}\{\rho_{\mathcal{H}_0+\Sigma}(t)\rho_{\mathcal{H}_0}(t)\}$$
$$=(2\pi\hbar)^d\int d\mathbf{r}\int d\mathbf{p}W_{\mathcal{H}_0+\Sigma}(\mathbf{r},\mathbf{p};t)W_{\mathcal{H}_0}(\mathbf{r},\mathbf{p};t). \tag{1.2}$$

We have used the standard definitions

$$\rho_{\mathcal{H}}=|\psi\rangle\langle\psi| \quad \text{with} \quad |\psi\rangle=e^{-i\mathcal{H}t/\hbar}|\psi_0\rangle, \tag{1.3}$$

$$W_{\mathcal{H}}(\mathbf{r},\mathbf{p};t)=\frac{1}{(2\pi\hbar)^d}\int d\delta\mathbf{r}\exp\left[-\frac{i}{\hbar}\mathbf{p}\cdot\delta\mathbf{r}\right]$$
$$\times\left\langle\mathbf{r}+\frac{\delta\mathbf{r}}{2}\middle|\rho_{\mathcal{H}}\middle|\mathbf{r}-\frac{\delta\mathbf{r}}{2}\right\rangle, \tag{1.4}$$

where d is the dimensionality of the space.

In consistency with the experimental behavior of the polarization echo, the LE of a classically chaotic one-body Hamiltonian $\mathcal{H}_0$ was found to exhibit an intrinsic decay rate.[18] This result is valid beyond some critical value of the perturbation. Interestingly, the decay rate is precisely the Lyapunov exponent λ of the classical system. A related relevance of the classical dynamics had been hinted from the analysis of the entropy growth of dissipative systems.[19]

The purely Hamiltonian character of the model of Ref. 18, as well as the result of a classical parameter λ governing a *bona fide* quantum property M, attracted considerable attention. A quite intense activity has been devoted in the last two years in order to test these predictions in various model systems and pursue further developments of the theory.[20–36]

The Lyapunov behavior has been numerically obtained in models of a Lorentz gas,[21] kicked tops,[22,23] Bunimovich stadium,[24] bath tube stadium,[25] and sawtooth map.[26] The analytical results have been mainly focused in the small perturbation region. Jacquod and collaborators[22] identified the regime below the critical perturbation as following a Fermi golden rule through the energy uncertainty produced by the perturbation which was also analyzed with semiclassical tools.[27] Prosen and collaborators[28,29] showed that $M(t)$ in the perturbative regime depends on the specific time dependence of the perturbation correlation functions. The transition between the perturbative Gaussian regime to the Fermi golden rule has also been studied using the semiclassical approximation as well as random matrix theory.[30]

The Lyapunov regime bears a clear signature of the underlying classical dynamics. Investigations on bounded systems[22,24] could not study the behavior of the LE after the Ehrenfest time (as defined by Berman and Zaslavsky[37]) because of the finite-size long-time saturation. This raises the question of whether the independence of the decay rate on the perturbation strength is a consequence of the quantum-classical correspondence principle. As we will analyze in this work, the situation is far less trivial. Using that the Lorentz gas is an extended system, we are going to show that this regime persists for times much larger than the Ehrenfest time. In addition, the quantum LE is functionally different than what a direct estimation would yield for the classical LE (for the chaotic,[18] as well as the integrable[31,32] cases). Moreover, the classical counterpart of the LE is problematic since a wide range of dynamic behaviors is obtained in different situations.[29,33,34]

The LE has also been studied in different disordered systems.[20,35] It has been shown in both cases that the long range of the perturbing potential, as emphasized in Ref. 18, is crucial in order to obtain a perturbation-independent regime.

The various approximations that the semiclassical theory of Ref. 18 relies on were further corroborated using an initial momentum representation of the wave packet.[36] This changes the sum over an uncontrolled number of trajectories into only one, which allows the exact numerical evaluation of the semiclassical expression for the echo.

Taking the perturbation as the action of an external environment allows us to think of the LE as a measure of the decoherence. This approach has been advocated by Zurek,[38] and later extended[39] by studying the decay of $M(t)$ as expressed by a product of Wigner functions [Eq. (1.2)]. A semiclassical approximation to the Wigner function allows us to separate the different contributions to the LE coming from classical and nonclassical processes. As we discuss in detail in the sequel, such distinction enables us to understand the relation to decoherence, and how it builds in until the classical terms finally dominate the LE.

With the goal of addressing experimentally relevant systems,[40–42] we illustrate our findings in a simple model with classical chaotic dynamics: the Lorentz gas. This system has been shown to exhibit a well-defined Lyapunov regime.[21] The semiclassical theory that we develop, as well as the extensive numerical results that we present in this work, allows us to establish and characterize the range where the perturbation-independent regime has the universality observed in classical chaos.

This universality manifests itself by the robustness of the Lyapunov regime with respect to various effects. First, in the semiclassical limit of the de Broglie wavelength λ_B going to zero, the borders of the regime extend from zero perturbation up to a classical upper bound. Second, and as stated above, for finite λ_B the Lyapunov regime extends up to times arbitrarily larger than Ehrenfest's time. Finally, universality is also evidenced by the insensitivity of the Lyapunov regime with respect to the form of the perturbation or the (nonaveraged) behavior of individual semiclassical initial conditions.

The paper is organized as follows. In Sec. II we develop the semiclassical approach to the LE with a quenched disorder playing the role of the perturbation, as proposed in Ref. 18. We then discuss the main assumptions and set the theoretical framework that will be further developed in the rest of the paper. In Sec. III we consider a specific model, the Lorentz gas. In this model we apply a completely different (although still global) perturbation than in the previous case, which allows us to study the dependence of the Lyapunov regime on the form of the perturbation. We first characterize the classical dynamics of the Lorentz gas, as well as that of the perturbation, and then present a semiclassical calculation of the LE, discussing the different regimes predicted by the theory. In Sec. IV we concentrate on the main results of this work. The universality of the Lyapunov regime is discussed

and supported with numerical results on the semiclassical limit, the behavior after the Ehrenfest time, and the effects of averaging. In Sec. V we discuss the relation of the LE to decoherence by studying the semiclassical approximation to the Wigner function and reinterpreting the results of Sec. II under this highlight. We conclude in Sec. VI with some final remarks.

II. THE LOSCHMIDT ECHO—SEMICLASSICAL ANALYSIS

A. Semiclassical evolution

In this section we calculate the Loschmidt echo [Eq. (1.1)] for a generic chaotic system $\mathcal{H}_0$ and a perturbation Σ arising from a quenched disorder. We follow the analytical scheme of Ref. 18, discussing the main assumptions and the generality of the results. We choose as initial state a Gaussian wave packet (of width σ), which is the closest we can get to a classical state:

$$\psi(\bar{\mathbf{r}},t=0)=\left(\frac{1}{\pi\sigma^2}\right)^{d/4}\exp\left[\frac{i}{\hbar}\mathbf{p}_0\cdot(\bar{\mathbf{r}}-\mathbf{r}_0)-\frac{1}{2\sigma^2}(\bar{\mathbf{r}}-\mathbf{r}_0)^2\right]. \tag{2.1}$$

We will keep the spatial dimension d arbitrary in the analytical calculations, but it will be fixed to $d=2$ for the numerical studies of Sec. IV. It has been shown[43] that if the initial state is a superposition of N Gaussians, the final result is the same exponential decay one obtains with a single Gaussian but normalized by N. Thus, our results will be valid only when the initial state can be decomposed as a sum of Gaussians. The exponential decay is observed also with momentum eigenstates,[26] but it is not universal for a random state or an eigenstate of the system.

The time evolution of the state $\psi(\bar{\mathbf{r}},0)$ is given by

$$\psi(\mathbf{r},t)=\int d\bar{\mathbf{r}}K(\mathbf{r},\bar{\mathbf{r}};t)\psi(\bar{\mathbf{r}},0), \tag{2.2}$$

with the propagator

$$K(\mathbf{r},\bar{\mathbf{r}};t)=\langle\mathbf{r}|e^{-i\mathcal{H}t/\hbar}|\bar{\mathbf{r}}\rangle. \tag{2.3}$$

We will use the semiclassical expansion of the propagator[44,45] as a sum over classical trajectories $s(\bar{\mathbf{r}},\mathbf{r},t)$, going from $\bar{\mathbf{r}}$ to $\mathbf{r}$ in a time t,

$$K(\mathbf{r},\bar{\mathbf{r}};t)=\sum_{s(\mathbf{r},\mathbf{r},t)}K_s(\mathbf{r},\bar{\mathbf{r}};t),$$

$$K_s(\mathbf{r},\bar{\mathbf{r}};t)=\left(\frac{1}{2\pi i\hbar}\right)^{d/2}C_s^{1/2}\exp\left[\frac{i}{\hbar}S_s(\mathbf{r},\bar{\mathbf{r}};t)-i\frac{\pi}{2}\mu_s\right], \tag{2.4}$$

valid in the limit of large energies for which the de Broglie wavelength $(\lambda_B=2\pi/k_F=2\pi\hbar/p_0)$ is the minimal length scale. $S_s(\mathbf{r},\bar{\mathbf{r}};t)=\int_0^t d\bar{t}L_s[\mathbf{q}_s(\bar{t}),\dot{\mathbf{q}}_s(\bar{t});\bar{t}]$ is the action over the trajectory s and L the Lagrangian. The Jacobian $C_s=|\det B_s|$ accounts for the conservation of classical probabilities, with the matrix

$$(B_s)_{ij}=-\frac{\partial^2 S_s}{\partial\mathbf{r}_i\partial\bar{\mathbf{r}}_j}, \tag{2.5}$$

obtained from the derivatives of the action with respect to the various components of the initial and final positions. We denote by μ_s the Maslov index, counting the number of conjugate points of the trajectory s. Since we will work with fairly concentrated initial wave packets, we use that $\nabla_{\mathbf{r}_i}\bar{S}_s|_{\mathbf{r}=\mathbf{r}_0}=-\bar{\mathbf{p}}_{s,i}$ ($\bar{\mathbf{p}}_{s,i}$ is the ith component of the initial momentum of the trajectory s) and we expand the action as

$$S_s(\mathbf{r},\bar{\mathbf{r}};t)\simeq S_{\hat{s}}(\mathbf{r},\mathbf{r}_0;t)-\bar{\mathbf{p}}_{\hat{s}}\cdot(\bar{\mathbf{r}}-\mathbf{r}_0). \tag{2.6}$$

We are led to work with trajectories $\hat{s}$ that join $\mathbf{r}_0$ to $\mathbf{r}$ in a time t, which are slightly modified with respect to the original trajectories $s(\bar{\mathbf{r}},\mathbf{r},t)$. We can therefore write

$$\begin{aligned}\psi(\mathbf{r},t)&=\sum_{s(\mathbf{r}_0,\mathbf{r},t)}K_s(\mathbf{r},\mathbf{r}_0;t)\int d\bar{\mathbf{r}}\exp\left[-\frac{i}{\hbar}\bar{\mathbf{p}}_s\cdot(\bar{\mathbf{r}}-\mathbf{r}_0)\right]\psi(\bar{\mathbf{r}},0)\\&=(4\pi\sigma^2)^{d/4}\sum_{s(\mathbf{r}_0,\mathbf{r},t)}K_s(\mathbf{r},\mathbf{r}_0;t)\\&\quad\times\exp\left[-\frac{\sigma^2}{2\hbar^2}(\bar{\mathbf{p}}_s-\mathbf{p}_0)^2\right],\end{aligned} \tag{2.7}$$

where we have neglected second-order terms of S in $(\bar{\mathbf{r}}-\mathbf{r}_0)$ since we assume that the initial wave packet is much larger than the de Broglie wavelength ($\sigma\gg\lambda_B$). Equation (2.7) shows that only trajectories with initial momentum $\bar{\mathbf{p}}_s$ closer than $\hbar/\sigma$ to $\mathbf{p}_0$ are relevant for the propagation of the wave packet.

B. Semiclassical Loschmidt echo

The amplitude of the Loschmidt echo, defined in Eq. (1.1), for the initial condition (2.1), can be approximated semiclassically as

$$\begin{aligned}m(t)&=\left(\frac{\sigma^2}{\pi\hbar^2}\right)^{d/2}\int d\mathbf{r}\sum_{s,\tilde{s}}C_s^{1/2}C_{\tilde{s}}^{1/2}\\&\quad\times\exp\left[\frac{i}{\hbar}(S_s-S_{\tilde{s}})-\frac{i\pi}{2}(\mu_s-\mu_{\tilde{s}})\right]\\&\quad\times\exp\left[-\frac{\sigma^2}{2\hbar^2}[(\bar{\mathbf{p}}_s-\mathbf{p}_0)^2+(\bar{\mathbf{p}}_{\tilde{s}}-\mathbf{p}_0)^2]\right].\end{aligned} \tag{2.8}$$

Without perturbation ($\Sigma=0$) and restricting ourselves to the terms with $s=\tilde{s}$ (which leaves aside terms with a highly oscillating phase) we simply have

$$m(t)=\left(\frac{\sigma^2}{\pi\hbar^2}\right)^{d/2}\int d\mathbf{r}\sum_{s(\mathbf{r}_0,\mathbf{r},t)} C_s\exp\left[-\frac{\sigma^2}{\hbar^2}(\overline{\mathbf{p}}_s-\mathbf{p}_0^2)^2\right]=1. \tag{2.9}$$

We have performed the change from the final position variable $\mathbf{r}$ to the initial momentum $\overline{\mathbf{p}}_s$ using the Jacobian C, and then carried out a simple Gaussian integration over the variable $\overline{\mathbf{p}}_s$.

For perturbations Σ that are classically weak (as not to change appreciably the trajectories governed by the dynamics of $\mathcal{H}_0$), we can also neglect the terms of Eq. (2.8) with $s\neq\tilde{s}$ and write

$$m(t)\simeq\left(\frac{\sigma^2}{\pi\hbar^2}\right)^{d/2}\int d\mathbf{r}\sum_s C_s\exp\left[\frac{i}{\hbar}\Delta S_s\right]\times\exp\left[-\frac{\sigma^2}{\hbar^2}[(\overline{\mathbf{p}}_s-\mathbf{p}_0)^2]\right], \tag{2.10}$$

where ΔS_s is the modification of the action, associated with the trajectory s, by the effect of the perturbation Σ. It can be obtained as

$$\Delta S_s=-\int_0^t d\overline{t}\,\overline{\Sigma}_s[\mathbf{q}(\overline{t}),\dot{\mathbf{q}}(\overline{t})], \tag{2.11}$$

in the case where the perturbation appears as a potential energy in the Hamiltonian (like we discuss in this chapter). If the perturbation is in the kinetic term of the Hamiltonian (such as in Sec. III), there is an irrelevant change of sign.

Clearly, individual classical trajectories will be exponentially sensitive to perturbations and the diagonal approximation of Eq. (2.10) would sustain only for logarithmically short times, rendering our following calculations useless. However, it has been argued[36] that this approximation is valid for much longer times because of the structural stability of the manifold of initial states that evolve classically.[27] This allows for the existence of trajectories arriving at $\mathbf{r}$ and departing exponentially close to $\mathbf{r}_0$.

Within the approximation of Eq. (2.10), the LE is expressed as a double integral containing two trajectories:

$$M(t)=\left(\frac{\sigma^2}{\pi\hbar^2}\right)^{d}\int d\mathbf{r}\int d\mathbf{r}'\sum_{s(\mathbf{r}_0,\mathbf{r},t)}\sum_{s'(\mathbf{r}_0,\mathbf{r}',t)} C_sC_{s'}\times\exp\left[\frac{i}{\hbar}(\Delta S_s-\Delta S_{s'})\right]\times\exp\left[-\frac{\sigma^2}{\hbar^2}[(\mathbf{p}_s-\mathbf{p}_0)^2+(\mathbf{p}_{s'}-\mathbf{p}_0)^2]\right]. \tag{2.12}$$

As in Ref. 18, we can decompose the LE as

$$M(t)=M^{\mathrm{nd}}(t)+M^{d}(t), \tag{2.13}$$

where the first term (nondiagonal) contains trajectories s and s' exploring different regions of phase space, while in the second (diagonal) s' remains close to s. Such a distinction is essential when considering the effect of the perturbation over the different contributions.

C. Quenched disorder as a perturbation

In order to calculate the different components to the LE [Eqs. (2.12) and (2.13)] we need to characterize the perturbation Σ. One possible choice[18] is a quenched disorder given by N_i impurities with a Gaussian potential characterized by the correlation length ξ,

$$\Sigma=\tilde{V}(\mathbf{r})=\sum_{\alpha=1}^{N_i}\frac{u_\alpha}{(2\pi\xi^2)^{d/2}}\exp\left[-\frac{1}{2\xi^2}(\mathbf{r}-\mathbf{R}_\alpha)^2\right]. \tag{2.14}$$

The independent impurities are uniformly distributed (at positions $\mathbf{R}_\alpha$) with density $n_i=N_i/V$, (V is the sample volume). The strengths u_α obey $\langle u_\alpha u_\beta\rangle=u^2\delta_{\alpha\beta}$. The correlation function of the above potential is given by

$$C_{\tilde{V}}(|\mathbf{q}-\mathbf{q}'|)=\langle\tilde{V}(\mathbf{q})\tilde{V}(\mathbf{q}')\rangle=\frac{u^2n_i}{(4\pi\xi^2)^{d/2}}\exp\left[-\frac{1}{4\xi^2}(\mathbf{q}-\mathbf{q}')^2\right]. \tag{2.15}$$

The perturbation (2.14) does not lead to the well-known physics of disordered systems, since the potential $\tilde{V}$ is not part of $\mathcal{H}_0$, but of Σ. Then, it acts only in the backward propagation of the LE setup. On the other hand, the analogy with standard disordered systems is very useful for the analytical developments. The finite range of the potential allows us to apply the semiclassical tool (provided $\xi k_F\gg 1$), as has been extensively used in the calculation of the orbital response of weak disordered quantum dots.[46–48] The finite range of the potential is a crucial ingredient in order to bridge the gap between the physics of disordered and dynamical systems[35,47] and to obtain the Lyapunov regime.[18] Moreover, taking a finite ξ is not only helpful for computational or conceptual purposes, but it constitutes an appropriate approximation for an uncontrolled error in the reversal procedure $\mathcal{H}_0\to-(\mathcal{H}_0+\Sigma)$ as well as an approximate description for an external environment. Without entering into a discussion about what kind of perturbation more appropriately represents an external environment, it is reasonable to admit that the interaction with the environment will not be local (or short range), but will extend over certain typical length.

As discussed in the preceding section, in the leading order of $\hbar$ and for sufficiently weak perturbations, we can neglect the changes in the classical dynamics associated with the disorder. We simply modify the contributions to the semiclassical expansion of the LE associated with a trajectory s (or in general to any quantity that can be expressed in terms of the propagators) by adding the extra phase ΔS of Eq. (2.11). For the perturbation (2.14) we can make the change of variables $\mathbf{q}=\mathbf{v}\overline{t}$ and write

$$\Delta S_s = -\frac{1}{v_0}\int_{\mathcal{C}_s^c} V(\mathbf{q})dq. \tag{2.16}$$

The integration is now over the unperturbed trajectory $\mathcal{C}_s^c$, and we have assumed that the velocity along the trajectory remains unchanged with respect to its initial value $v_0 = p_0/m = L_s/t$.

For trajectories of length $L_s \gg \xi$, the contributions to ΔS from segments separated more than ξ are uncorrelated. The stochastic accumulation of action along the path can be therefore interpreted as determined by a random-walk process, resulting in a Gaussian distribution of $\Delta S_s(L_s)$. This has also been verified numerically in Ref. 36. The ensemble average over the propagator (2.4) [or over independent trajectories in Eq. (2.12)] is then obtained from

$$\left\langle \exp\left[\frac{i}{\hbar}\Delta S_s\right]\right\rangle = \exp\left[-\frac{\langle \Delta S_s^2\rangle}{2\hbar^2}\right], \tag{2.17}$$

and therefore entirely specified by the variance

$$\langle \Delta S_s^2\rangle = \frac{1}{v_0^2}\int_{\mathcal{C}_s^c} dq \int_{\mathcal{C}_s^c} dq' \langle V(\mathbf{q})V(\mathbf{q}')\rangle. \tag{2.18}$$

Since the length L_s of the trajectory is supposed to be much larger than ξ, the integral over $q-q'$ can be taken from $-\infty$ to $+\infty$, while the integral on $(q+q')/2$ gives a factor of L_s. We thus have

$$\langle \Delta S^2\rangle = \frac{L_s}{v_0^2}\int dq C(\mathbf{q}), \tag{2.19}$$

resulting in

$$\left\langle \exp\left[\frac{i}{\hbar}\Delta S_s\right]\right\rangle = \exp\left[-\frac{L_s}{2\tilde{\ell}}\right] = \exp\left[-\frac{v_0 t}{2\tilde{\ell}}\right]. \tag{2.20}$$

In analogy with disordered systems,[46,47] we have defined the typical length over which the quantum phase is modified by the perturbation as

$$\frac{1}{\tilde{\ell}} = \frac{1}{\hbar^2 v_0^2}\int dq C(\mathbf{q}) = \frac{u^2 n_i}{v_0^2 \hbar^2 (4\pi\xi^2)^{(d-1)/2}}. \tag{2.21}$$

The "elastic mean free path" $\tilde{\ell}$ and the mean free time $\tilde{\tau} = \tilde{\ell}/v_0$ associated with the perturbation[49] will constitute a measure of the strength of the coupling.

Taking impurity averages is technically convenient, but not crucial. Results like that of Eq. (2.20) would also arise from considering a single-impurity configuration and a large number of trajectories exploring different regions of phase space.

D. Loschmidt echo in a classically chaotic system

Once we have settled the hypothesis with respect to the perturbation, we can go back to Eqs. (2.12) and (2.13) to calculate the two contributions to the Loschmidt echo.

In the nondiagonal term the impurity average can be done independently for s and s', since the two trajectories explore different regions of phase space. Therefore, upon impurity average the nondiagonal term becomes

$$M^{\mathrm{nd}}(t) = |\langle m(t)\rangle|^2 = \left(\frac{\sigma^2}{\pi\hbar^2}\right)^d \left| \int d\mathbf{r} \sum_s C_s \times \exp\left[-\frac{\sigma^2}{\hbar^2}(\bar{\mathbf{p}}_s - \mathbf{p}_0)^2\right] \left\langle \exp\left[\frac{i}{\hbar}\Delta S_s\right]\right\rangle \right|^2. \tag{2.22}$$

We have kept the same notation for the averaged and individual LE, in order to simplify the notation, and because it will be demonstrated that this distinction is not crucial. According to Eq. (2.20) we have[18]

$$M^{\mathrm{nd}}(t) = \left(\frac{\sigma^2}{\pi\hbar^2}\right)^d \exp\left[-\frac{v_0 t}{\tilde{\ell}}\right] \left| \int d\mathbf{r} \sum_s C_s \times \exp\left[-\frac{\sigma^2}{\hbar^2}(\bar{\mathbf{p}}_s - \mathbf{p}_0)^2\right] \right|^2 = \exp\left[-\frac{v_0 t}{\tilde{\ell}}\right]. \tag{2.23}$$

This term depends on the perturbation, through $\tilde{\ell}$, and can be interpreted as a Fermi golden rule result.[22]

In the diagonal term the trajectories s and s' of Eq. (2.12) remain close to each other. The existence of such types of trajectories is based on the structural stability of the manifold[27,36] (opposed to the exponential sensitivity of individual trajectories). The actions ΔS_s and $\Delta S_{s'}$ accumulated by effect of the perturbation cannot be taken as uncorrelated, like in the previous case. A special treatment should be applied to the terms arising from $s \simeq s'$. The small difference between s and s' is only considered through the difference of actions, and therefore

$$M^d(t) = \left(\frac{\sigma^2}{\pi\hbar^2}\right)^d \int d\mathbf{r} \int d\mathbf{r}' \sum_s C_s^2 \exp\left[-\frac{2\sigma^2}{\hbar^2}(\bar{\mathbf{p}}_s - \mathbf{p}_0)^2\right] \times \left\langle \exp\left[\frac{i}{\hbar}(\Delta S_s - \Delta S_{s'})\right]\right\rangle. \tag{2.24}$$

Since s and s' are nearby trajectories, we can write

$$\Delta S_s - \Delta S_{s'} = \int_0^t d\bar{t}\ \nabla \tilde{V}(\mathbf{q}_s(\bar{t}))\cdot[\mathbf{q}_s(\bar{t}) - \mathbf{q}_{s'}(\bar{t})]. \tag{2.25}$$

The difference between the intermediate points of both trajectories can be expressed using the matrix B of Eq. (2.5):

$$\mathbf{q}_s(\bar{t}) - \mathbf{q}_{s'}(\bar{t}) = B^{-1}(\bar{t})(\bar{\mathbf{p}}_s - \bar{\mathbf{p}}_{s'}) = B^{-1}(\bar{t})B(t)(\mathbf{r}-\mathbf{r}'). \tag{2.26}$$

In the chaotic case the behavior of $B^{-1}(\bar{t})$ is dominated by the largest eigenvalue $e^{\lambda \bar{t}}$. Therefore we make the simplification $B^{-1}(\bar{t})B(t)=\exp[\lambda(\bar{t}-t)]I$, where I is the unit matrix and λ the mean Lyapunov exponent. Here, we use our hypothesis of strong chaos which excludes marginally stable regions[50] with anomalous time behavior. Assuming a Gaussian distribution for the random variable $\Delta S_s-\Delta S_{s'}$, in analogy with Eq. (2.17), we have

$$\left\langle \exp\left[\frac{i}{\hbar}(\Delta S_s-\Delta S_{s'})\right]\right\rangle = \exp\left[-\frac{1}{2\hbar^2}\int_0^t d\bar{t}\int_0^t d\bar{t}'\exp[\lambda(\bar{t}+\bar{t}'-2t)] \times C_{\nabla\tilde{V}}[|q_s(\bar{t})-q_s(\bar{t}')|](\mathbf{r}-\mathbf{r}')^2\right]. \tag{2.27}$$

Unlike the nondiagonal case, which was obtained through the correlation potential [Eq. (2.15)], we are now led to consider the "force correlator"

$$C_{\nabla\tilde{V}}(|\mathbf{q}-\mathbf{q}'|)=\langle\nabla\tilde{V}(\mathbf{q})\cdot\nabla\tilde{V}(\mathbf{q}')\rangle = \frac{u^2 n_i}{(4\pi\xi^2)^{d/2}}\left[\frac{d}{2\xi^2}-\left(\frac{\mathbf{q}-\mathbf{q}'}{2\xi^2}\right)^2\right] \times\exp\left[-\frac{1}{4\xi^2}(\mathbf{q}-\mathbf{q}')^2\right]. \tag{2.28}$$

Using the fact that $C_{\nabla\tilde{V}}$ is short ranged (in the scale of ξ), and working in the limit $\lambda t\gg 1$, the integrals of Eq. (2.27) yield

$$\left\langle \exp\left[\frac{i}{\hbar}(\Delta S_s-\Delta S_{s'})\right]\right\rangle=\exp\left[-\frac{A}{2\hbar^2}|\mathbf{r}-\mathbf{r}'|^2\right] \tag{2.29}$$

with

$$A=\frac{(d-1)u^2 n_i}{4\lambda v_0\xi^2(4\pi\xi^2)^{(d-1)/2}}. \tag{2.30}$$

Therefore, we have

$$M^d(t)=\left(\frac{\sigma^2}{\pi\hbar^2}\right)^d\int d\mathbf{r}\int d\mathbf{r}'\sum_s C_s^2 \times\exp\left[-\frac{2\sigma^2}{\hbar^2}(\bar{\mathbf{p}}_s-\mathbf{p}_0)^2\right]\exp\left[-\frac{A}{2\hbar^2}(\mathbf{r}-\mathbf{r}')^2\right].$$

A Gaussian integration over $(\mathbf{r}-\mathbf{r}')$ results in

$$M^d(t)=\left(\frac{\sigma^2}{\pi\hbar^2}\right)^d\int d\mathbf{r}\sum_s C_s^2\left(\frac{2\pi\hbar^2}{A}\right)^{d/2} \times\exp\left[-\frac{2\sigma^2}{\hbar^2}(\bar{\mathbf{p}}_s-\mathbf{p}_0)^2\right].$$

The factor C_s^2 reduces to C_s when we make the change of variables from $\mathbf{r}$ to $\bar{\mathbf{p}}$. In the long-time limit $C_s^{-1}\propto e^{\lambda t}$, while for short times $C_s^{-1}=(t/m)^d$. Using a form that interpolates between these two limits we have

$$M^d(t)=\left(\frac{\sigma^2}{\pi\hbar^2}\right)^d\int d\bar{\mathbf{p}}\left(\frac{2\pi\hbar^2}{A}\right)^{d/2}\left(\frac{m}{t}\right)^d\exp[-\lambda t] \times\exp\left[-\frac{2\sigma^2}{\hbar^2}(\bar{\mathbf{p}}-\mathbf{p}_0)^2\right] =\bar{A}\exp[-\lambda t], \tag{2.31}$$

with $\bar{A}=[\sigma m/(A^{1/2}t)]^d$. Since the integral over $\bar{\mathbf{p}}$ is concentrated around $\mathbf{p}_0$, the exponent λ is taken as the phase-space average value on the corresponding energy shell. The coupling Σ appears only in the prefactor (through $\bar{A}$) and therefore its detailed description is not crucial in discussing the time dependence of M^d.

The limits of small t and weak Σ yield an infinite $\bar{A}$, and thus a divergence in Eq. (2.31). However, our calculations are only valid in certain intervals of t and strength of the perturbation. The times considered should verify $v_0 t/\tilde{\ell}\geqslant 1$. Very long times, resulting in the failure of our diagonal approximations [Eqs. (2.12) and (2.24)] or our assumption that the trajectories are unaffected by the perturbation, are excluded from our analysis. Similarly, the small values of Σ are not properly treated in the semiclassical calculation of the diagonal term $M^d(t)$, while for strong Σ the perturbative treatment of the actions is expected to break down and the trajectories are affected by the quenched disorder. This last condition translates into a "transport mean free path"[46,47] $\tilde{\ell}_{\rm tr}=4(k\xi)^2\tilde{\ell}$ much larger than the typical dimension R of our system. In the limit $k\xi\gg 1$ that we are working with, we are able to verify the condition $\tilde{\ell}_{\rm tr}\gg R\gg\tilde{\ell}$.

Within the above limits, our semiclassical approach made it possible to estimate the two contributions of Eq. (2.13) to $M(t)$. The nondiagonal component $M^{\rm nd}(t)$ will dominate in the limit of small t or Σ. In particular, such a contribution ensures that $M_{\Sigma=0}(t)=1$ [see Eq. (2.9)], and that $M_\Sigma(t=0)=1$. The diagonal term will dominate over the nondiagonal one for perturbations strong enough to verify

$$\tilde{\ell}<\frac{v_0}{\lambda}. \tag{2.32}$$

This crossover condition is extremely important, and will be discussed in detail in the sequel.

It is worth noting that the width σ of the initial wave packet appears as a prefactor of the diagonal contribution. The nondiagonal term, on the other hand, is independent on

the initial wave packet. Therefore, as explained in Ref. 43, changing our initial state (2.1) into a coherent superposition of N wave packets would reduce M^d by a factor of N without changing M^{nd}. The localized character of the initial state is then a key ingredient in order to obtain the universal behavior. In particular, only a Fermi golden rule regime is observed when the initial state is random[23] or an eigenstate of $\mathcal{H}_0$.[51]

III. LOSCHMIDT ECHO IN THE TWO-DIMENSIONAL LORENTZ GAS

A. Classical dynamics of $\mathcal{H}_0$

We consider in this section the case where the system Hamiltonian $\mathcal{H}_0$ represents a two-dimensional Lorentz gas, i.e., a particle that moves freely (with speed v) between elastic collisions (with specular reflections) on an irregular array of hard-disk scatterers (impurities) of radius R. Such a billiard system is a paradigm of classical dynamics, and has been proven to exhibit mixing and ergodic behavior, while its dynamics for long distances is diffusive.[52–54] The existence of rigorous results for the Lorentz gas has made it a preferred playground to study the emergence of irreversible behavior out of the reversible laws of classical dynamics.[53] Moreover, antidot lattices defined in a two-dimensional electron gas,[40,41] or in acoustic and microwave cavities,[42] constitute an experimentally realizable quantum system where classical features have been identified and measured. We will use the terms antidot, impurity, and disk indistinctly.

In our numerical simulations we are limited to finite systems, therefore we will work in a square billiard of area L^2 (with N scatterers), and impose periodic boundary conditions. The concentration of disks is

$$c = N\pi R^2/L^2. \tag{3.1}$$

We require that each scatterer has an exclusion region R_{e} from its border, such that the distance between the centers of any pair of disks is larger than a value $2R_{\mathrm{e}} > 2R$. Such a requirement is important to avoid the trapping of the classical particle and the wave-function localization in the quantum case. The antidots density is set to be roughly uniform, and the concentration is chosen to be the largest one compatible with the value of R_{e}, obtained numerically as $c = 0.7\pi R^2/4R_{\mathrm{e}}^2$.

The Lorentz gas has been thoroughly studied,[53] and we will not discuss here its classical dynamics in detail. We will simply recall some of its properties that will be used in the sequel, and present the numerical simulations that allow us to extract some important physical parameters.

The chaotic character of the dynamics is a consequence of the defocusing nature of the collisions. The separation between a particle with impact parameter x and a second one with impact parameter $x+\delta x$ that have traveled a distance s after a collision will grow as (see Fig. 1)

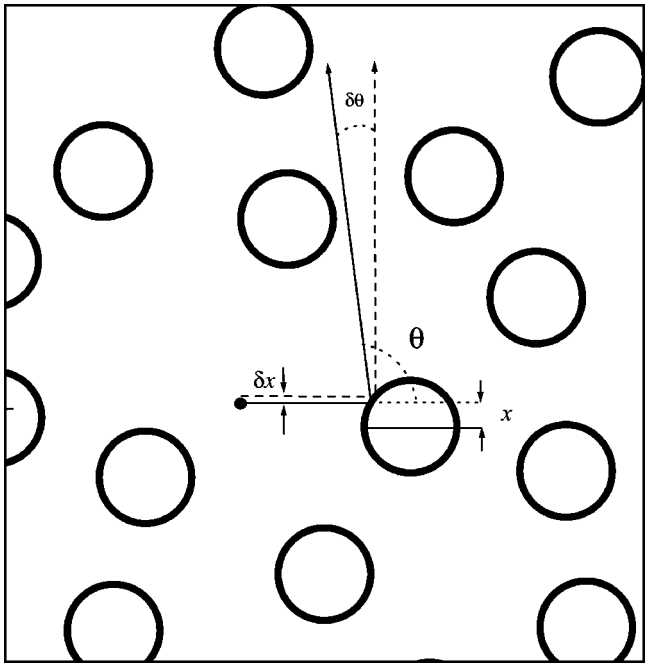

FIG. 1. Schematics of a Lorentz gas showing the dispersion of two trajectories initially close to each other (with a difference δx in the impact parameter x). The angle $\delta\theta$ between the two trajectories increases after each collision as described in the text.

$$\delta d \simeq \delta x + \delta\theta s \simeq \delta x\left(1 + \frac{2s}{\sqrt{R^2 - x^2}}\right). \tag{3.2}$$

The next collision will further amplify the separation, due to the new impact parameters and the different incidence angles.

Within the above restrictions, the exclusion distance R_{e} completely determines the dynamical properties of the Lorentz gas. Among them, we are interested in the Lyapunov exponent (measuring the rate of separation of two nearby trajectories), the elastic mean free path ℓ (given by the typical distance between two collisions), and the transport mean free path ℓ_{tr} (defined as the distance over which the momentum is randomized and the dynamics can be taken as effectively diffusive).

A shifted Poisson distribution

$$P(s) = \begin{cases} \dfrac{\exp\{-s/[\ell - 2(R_{\mathrm{e}} - R)]\}}{[\ell - 2(R_{\mathrm{e}} - R)]\exp\{-2(R_{\mathrm{e}} - R)/[\ell - 2(R_{\mathrm{e}} - R)]\}} & \text{if } s > 2(R_{\mathrm{e}} - R) \\ 0 & \text{if } s < 2(R_{\mathrm{e}} - R) \end{cases} \tag{3.3}$$

is a reasonable guess for the distribution of lengths between successive collisions, which yields $\langle s\rangle = \ell = v\tau_e$, and is consistent with numerical simulations in the range of antidot concentration that we are interested in. Within this billiard model, the magnitude of the velocity and momentum are constants of motion, which we denote by v and p, respectively.

The elastic mean free path that we obtain numerically compares favorably with a simple estimation of the mean free distance in a strip of length L and width $2R$ with $2cL/\pi R$ disks,

$$\ell \simeq \frac{\pi R}{2c} - \frac{\pi R}{2} = \frac{R_e^2}{0.35R} - \frac{\pi R}{2}. \tag{3.4}$$

The diffusive character of the Lorentz gas can be put in evidence from the time evolution of the root-mean-square displacement over a collection of initial conditions. We numerically obtain $\langle r^2\rangle = 2dD\tau_{tr}$ (with $d=2$). $\tau_{tr} = \ell_{tr}/v$ is the mean time required to randomize the direction and $D = v\ell_{tr}/2d$ is the diffusion coefficient. The difference between ℓ and ℓ_{tr} arises from the angular dependence of the scattering cross section. Taking this factor into account we obtain a ratio ℓ_{tr}/ℓ which is in good agreement with the one obtained from the independently determined ℓ and ℓ_{tr}.

Various estimations of the Lyapunov exponent of the Lorentz gas are known. Considering the three-disk problem, Gaspard and Nicolis[55] obtained

$$\lambda = \frac{v}{2R_e - 2R} \ln\left[\frac{2R_e - R + (4R_e^2 - 4R_eR)^{1/2}}{R}\right]. \tag{3.5}$$

Considering a periodic Lorentz gas (repeated Sinai billiard) Laughlin proposed the form[10]

$$\lambda = \frac{v}{\ell} \ln\left[1 + \frac{\beta\ell}{R}\right], \tag{3.6}$$

where β is a geometrical factor of order 1. In the diluted limit ($c \ll 1$), van Beijeren and Dorfman[56] showed that

$$\lambda = 2\frac{N}{L^2} Rv \left(1 - \ln 2 - 0.577 - \ln\left[\frac{NR^2}{L^2}\right]\right). \tag{3.7}$$

Numerically, we use the procedure of Benettin *et al.*[57] to obtain the Lyapunov exponents. Two nearby trajectories are followed, and their separation is scaled down to the initial value δx_0 after a characteristic time t (which we take to be larger than the collision time). The Lyapunov exponent results from the average over the expanding rates in the different intervals:

$$\lambda = \lim_{n\to\infty} \frac{v}{n} \sum_{j=1}^{n} \frac{1}{s_j} \ln\left[\frac{\delta x_j}{\delta x_0}\right], \tag{3.8}$$

where s_j is the length of the jth interval and δx_j the separation just before the normalization. Technically, we should work with distances in phase space, rather than in configuration space, but the local instability makes this precision unnecessary.

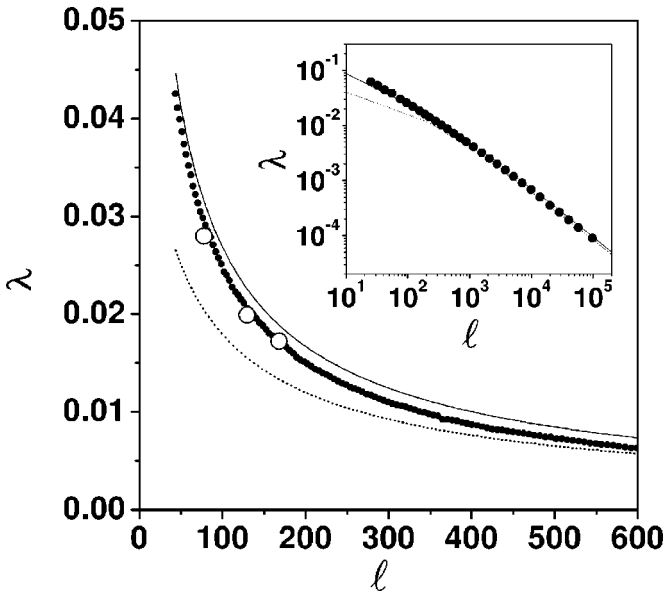

FIG. 2. Lyapunov exponent λ of the Lorentz gas as a function of the mean free path ℓ. The black dots represent our numerical values and the solid line the analytical estimate of Eq. (3.10). The dashed line indicates Laughlin's approximation [Eq. (3.6)] and the open dots are the quantum values obtained from the decay of the LE (Fig. 4 in the sequel). Inset: the same plot in log-log scale highlighting the agreement between the different approximations in the region of very small concentrations (large ℓ).

Benettin's algorithm can also be used for a semianalytical calculation of the Lyapunov exponent. Taking the length distribution of Eq. (3.3) to obtain the average separation after a collision from Eq. (3.2), and identifying the average over pieces of the trajectory with a geometrical average over impact parameters, we can write

$$\lambda = \frac{v}{R\ell} \int_0^R dx \ln\left[1 + \frac{2\ell}{\sqrt{R^2 - x^2}}\right]. \tag{3.9}$$

Performing the integration yields

$$\frac{\lambda}{v} = \frac{1}{\ell}\ln\left[\frac{\ell}{R}\right] + \frac{\pi}{R} + \sqrt{\frac{4}{R^2} - \frac{1}{\ell^2}}\left(\arcsin\left[\frac{R}{2\ell}\right] - \frac{\pi}{2}\right). \tag{3.10}$$

As shown in Fig. 2, the above expression reproduces remarkably well the numerical calculations of the Lyapunov exponent. It agrees also with the result of van Beijeren and Dorfman in the dilute limit, and gives good agreement with Laughlin's estimation.

B. Perturbation Hamiltonian

In Sec. II C we studied the case of a quenched disorder perturbation as in Ref. 18. In order to shed light on the dependence of the results on the details of the perturbation, we

consider a radically different perturbation for the case of the Lorentz gas: a distortion of the mass tensor introduced in Ref. 21, and briefly discussed in the sequel.

The isotropic mass tensor of $\mathcal{H}_0$, of diagonal components m_0, can be distorted by introducing an anisotropy such that $m_{xx}=m_0(1+\alpha)$ and $m_{yy}=m_0/(1+\alpha)$. This perturbation is inspired by the effect of a slight rotation of the sample in the problem of dipolar spin dynamics,[58] which modifies the mass of the spin-wave excitations. The kinetic part of the Hamiltonian is now affected by the perturbation, which is written as

$$\Sigma(\alpha)=\alpha\frac{p_y^2}{2m_0}-\frac{\alpha}{1+\alpha}\frac{p_x^2}{2m_0}. \tag{3.11}$$

In our analytical work we will stay within the leading-order perturbation in α. That is,

$$\Sigma(\alpha)=\frac{\alpha}{2m_0}(p_y^2-p_x^2). \tag{3.12}$$

Making the particle ''heavier'' in the x direction (i.e., we consider a positive α) modifies the equations of motion without changing the potential part of the Hamiltonian. It is important to notice that, unlike the case of quenched disorder, the perturbation (3.11) is nonrandom, and will not be able to provide any averaging procedure by itself, but through the underlying chaotic dynamics.

Numerical simulations of the evolution of two trajectories with the same initial conditions, the first one governed by $\mathcal{H}_0$ and the second one by $\mathcal{H}_0+\Sigma$, show that the distance in phase space grows exponentially with the same Lyapunov exponent that amplifies initial distances. The classical dynamics is then equally sensitive to changes in the Hamiltonian as to changes in the initial conditions.[59]

For a hard wall model, such as the one we are considering, the perturbation (3.11) is equivalent to having nonspecular reflections. One can resort to the minimum-action principle (see Appendix A) to obtain a generalized reflection law:

$$v_x'=\frac{v_x(m_xn_y^2-m_yn_x^2)-2v_ym_yn_xn_y}{m_xn_y^2+m_yn_x^2}, \tag{3.13a}$$

$$v_y'=\frac{v_y(m_yn_x^2-m_xn_y^2)-2v_xm_xn_xn_y}{m_xn_y^2+m_yn_x^2}, \tag{3.13b}$$

where v_x' and v_y' are the two components of the velocity after a collision against a surface defined by its normal unitary vector (n_x,n_y). Equations (3.13) allow us to show that the distortion of the mass tensor is equivalent to an area conserving deformation of the boundaries as $x\to x(1+\xi)$, $y\to y/(1+\xi)$, as used in other works on the LE,[24] where $\xi=\sqrt{1+\alpha}-1$ is the stretching parameter.

C. Semiclassical Loschmidt echo

We calculate in this chapter the Loschmidt echo for the system whose classical counterpart was previously discussed; $\mathcal{H}_0$ describes a Lorentz gas and Σ is given by Eq. (3.11). We adapt to the present perturbation the semiclassical approach of Sec. II and Ref. 18. As before, we take as initial state a Gaussian wave packet of width σ [Eq. (2.1)].

The semiclassical approach to the LE under a weak perturbation Σ is given by Eq. (2.12), with the extra phase

$$\Delta S_s=\int_0^t d\bar{t}\,\bar{\Sigma}_s(\mathbf{q}(\bar{t}),\dot{\mathbf{q}}(\bar{t})). \tag{3.14}$$

The sign difference with Eq. (2.11) results because the perturbation is now in the kinetic part of the Hamiltonian. On the other hand, as explained before, this sign turns out to be irrelevant.

With the perturbation of Eq. (3.12) we have to integrate a piecewise constant function (in between collisions with the scatterers), obtaining

$$\Delta S_s=\frac{\alpha m_0}{2}\sum_{i=1}^{N_s}\tau_i(2v_{y_i}^2-v^2). \tag{3.15}$$

We have used $v_x^2+v_y^2=v^2$, and have defined τ_i as the free time of flight ending with the ith collision, v_{y_i} is the y component of the velocity in such an interval, and N_s as the number of collisions that the trajectory s suffers during the time t.

As we saw in Sec. III A, the time of flight τ_i (or the inter-collision length $v\tau_i$) has a shifted Poisson distribution [Eq. (3.3)]. This observation will turn out to be important in the analytical calculations that follow since the sum of Eq. (3.15) for a long trajectory can be taken as composed of uncorrelated random variables following the above-mentioned distribution. Unlike the case of Sec. II, the randomness is not associated with the perturbation (which is fixed), but with the diffusive dynamics generated by $\mathcal{H}_0$.

D. Nondiagonal contribution

As in the case of Sec. II, the nondiagonal contribution is given by the second moment

$$\langle\Delta S_s^2\rangle=\frac{\alpha^2m_0^2}{4}\left\langle\sum_{i,j=1}^{N_s}\tau_i\tau_j(2v_{y_i}^2-v^2)(2v_{y_j}^2-v^2)\right\rangle. \tag{3.16}$$

Separating in diagonal ($i=j$) and nondiagonal ($i\neq j$) contributions (in pieces of trajectory) we have

$$\langle\Delta S_s^2\rangle=\frac{\alpha^2m_0^2N_s}{4}[\langle\tau_i^2\rangle(4\langle v_{y_i}^4\rangle-4v^2\langle v_{y_i}^2\rangle+v^4)+(N_s-1)\langle\tau_i\rangle^2(4\langle v_{y_i}^2\rangle^2-4v^2\langle v_{y_i}^2\rangle+v^4)]. \tag{3.17}$$

We have assumed that different pieces of the trajectory ($i\neq j$) are uncorrelated, and that within a given piece i, τ_i and v_{y_i} are also uncorrelated. According to the distribution of times of flight (3.3) we have

$$\langle\tau\rangle=\tau_e, \tag{3.18a}$$

$$\langle \tau^2 \rangle = 2\tau_e^2. \tag{3.18b}$$

Assuming that the velocity distribution is isotropic [$P(\theta) = 1/2\pi$, where θ is the angle of the velocity with respect to a fixed axis] is in good agreement with our numerical simulations, and results in

$$\langle v_y^2 \rangle = v^2 \langle \sin^2\theta \rangle = \frac{v^2}{2}, \tag{3.19a}$$

$$\langle v_y^4 \rangle = v^4 \langle \sin^4\theta \rangle = \frac{3v^4}{8}. \tag{3.19b}$$

We thus obtain that $4\langle v_{y_i}^2 \rangle^2 - 4v^2\langle v_{y_i}^2 \rangle + v^4 = 0$, implying a cancellation of the cross terms of $\langle \Delta S_s^2 \rangle$, consistently with the lack of correlations between different pieces that we have assumed. We therefore have

$$\langle \Delta S_s^2 \rangle = \frac{\alpha^2 m_0^2 N_s \tau_e^2 v^4}{4}. \tag{3.20}$$

For a given t, N_s is also a random variable, but for $t \gg \tau_e$ we can approximate it by its mean value t/τ_e and write

$$\langle \Delta S_s^2 \rangle = \frac{\alpha^2 m_0^2 v^4 \tau_e t}{4}. \tag{3.21}$$

We therefore have for the average echo amplitude

$$\begin{aligned}\langle m(t) \rangle &\simeq \exp\left[-\frac{\alpha^2 m_0^2 v^4 \tau_e t}{8\hbar^2} \right] \left(\frac{\sigma^2}{\pi\hbar^2} \right)^{d/2} \int d\mathbf{r} \sum_s C_s \\ &\times \exp\left[-\frac{\sigma^2}{\hbar^2} (\overline{\mathbf{p}}_s - \mathbf{p}_0)^2 \right] \\ &= \exp\left[-\frac{vt}{2\tilde{\ell}} \right],\end{aligned} \tag{3.22}$$

where we have again used C_s as a Jacobian of the transformation from $\mathbf{r}$ to $\overline{\mathbf{p}}_s$ and we have defined an effective mean free path of the perturbation by

$$\frac{1}{\tilde{\ell}} = \frac{m_0^2 v^2 \ell}{4\hbar^2} \alpha^2. \tag{3.23}$$

The effective mean free path $\tilde{\ell} = v\,\tilde{\tau}$ should be distinguished from $\ell = v\tau_e$ since the former is associated to the dynamics of Σ and $\mathcal{H}_0$, while the latter is only fixed by $\mathcal{H}_0$. Obviously, our results are only applicable in the case of a weak perturbation verifying $\tilde{\ell} \gg \ell$. From Eq. (3.22) we obtain the nondiagonal component of the LE as

$$M^{\mathrm{nd}}(t) = |\langle m(t) \rangle|^2 = \exp\left[-\frac{vt}{\tilde{\ell}} \right]. \tag{3.24}$$

In the following sections we study the conditions under which the correlations not contained in the FGR approximation dominate the LE, while in Sec. IV we will test the above results against numerical simulations.

E. Diagonal contribution

As in Sec. II, we have to discuss separately the contribution to the LE [Eq. (2.12)] originated by pairs of trajectories s and s' that remain close to each other. In that case the terms ΔS_s and $\Delta S_{s'}$ are not uncorrelated. The corresponding diagonal contribution to the LE is given by Eq. (2.24), and then we have to calculate the extra actions for $s \simeq s'$. As in Fig. 1, we represent by θ ($\theta + \delta$) the angle of the trajectory s (s') with a fixed direction (i.e., that of the x axis). We can then write the perturbation [Eq. (3.11)] for each trajectory as

$$\Sigma_s = \frac{\alpha}{2m_0} p^2 (2\sin^2\theta - 1), \tag{3.25a}$$

$$\Sigma_{s'} = \frac{\alpha}{2m_0} p^2 (2\sin^2\theta - 2\delta \sin 2\theta - 1) + \mathcal{O}(\delta^2). \tag{3.25b}$$

Assuming that the time of flight τ_i is the same for s and s' we have

$$\Delta S_s - \Delta S_{s'} = \frac{\alpha p^2}{m_0} \int_0^t d\bar{t}\, \delta(\bar{t}) \sin[2\theta(\bar{t})]. \tag{3.26}$$

The angles δ alternate in sign, but the exponential divergence between nearby trajectories allows one to approximate the angle difference after n collisions as $|\delta_n| = |\delta_1| e^{\lambda n \tau_e}$. A detailed analysis of the classical dynamics shows that the distance between the two trajectories grows with the number of collisions as $d_1 = |\delta_1| v\tau_1$, $d_2 = d_1 + |\delta_2| v\tau_2$, and therefore

$$\begin{aligned} d_{N_s} &\simeq v \sum_{j=1}^{N_s} |\delta_j| \tau_j \simeq v\tau_e |\delta_1| \sum_{j=1}^{N_s} e^{(j-1)\lambda\tau_e} \\ &= \ell |\delta_1| \frac{e^{N_s \lambda \tau_e} - 1}{e^{\lambda\tau_e} - 1}. \end{aligned} \tag{3.27}$$

By eliminating $|\delta_1|$ we can express an intermediate angle $\delta(\bar{t})$ as a function of the final separation $|\mathbf{r} - \mathbf{r}'| = d_{N_s}$,

$$\delta(\bar{t}) \simeq \frac{|\mathbf{r} - \mathbf{r}'|}{\ell} \frac{e^{\lambda\tau_e} - 1}{e^{\lambda t} - 1} e^{\lambda \bar{t}}, \tag{3.28}$$

where again we have used that $t = N_s \tau_e$ is valid on average. Assuming that the action difference is a Gaussian random variable, in the evaluation of Eq. (2.24) we only need its second moment

$$\langle(\Delta S_s-\Delta S_{s'})^2\rangle \simeq \alpha^2 m_0^2 v^4 \frac{|\mathbf{r}-\mathbf{r}'|^2}{\ell^2}\left(\frac{e^{\lambda\tau_e}-1}{e^{\lambda t}-1}\right)^2 \times\left\langle \int_0^t d\bar{t}\int_0^t d\bar{t}' e^{\lambda\bar{t}+\lambda\bar{t}'}\sin[2\theta(\bar{t})]\sin[2\theta(\bar{t}')]\right\rangle. \tag{3.29}$$

As before, we assume that the different pieces are uncorrelated and the angles θ_i uniformly distributed. Therefore $\langle\sin[2\theta_i]\sin[2\theta_j]\rangle=\delta_{ij}/2$ and

$$\begin{aligned}\langle(\Delta S_s-\Delta S_{s'})^2\rangle &\simeq \frac{\alpha^2}{2}\left(\frac{m_0v^2}{\ell}\right)^2|\mathbf{r}-\mathbf{r}'|^2\left(\frac{e^{\lambda\tau_e}-1}{e^{\lambda t}-1}\right)^2 \times\sum_{i=1}^{N_s}\left\langle\int_{t_{i-1}}^{t_i} d\bar{t}e^{\lambda\bar{t}}\right\rangle^2 \\ &=\frac{\alpha^2}{2}\left(\frac{m_0v^2}{\lambda\ell}\right)^2|\mathbf{r}-\mathbf{r}'|^2\frac{(e^{\lambda\tau_e}-1)^4}{(e^{\lambda t}-1)^2}\frac{e^{2\lambda N_s\tau_e}-1}{e^{2\lambda\tau_e}-1} \\ &=A|\mathbf{r}-\mathbf{r}'|^2,\end{aligned} \tag{3.30}$$

where we have taken the limit $\lambda t\gg 1$, and defined

$$A=\frac{\alpha^2}{2}\left(\frac{m_0v^2}{\lambda\ell}\right)^2\frac{(e^{\lambda\tau_e}-1)^3}{e^{\lambda\tau_e}+1}. \tag{3.31}$$

Our result (3.30) is analogous to Eq. (2.29) obtained in the case of a perturbation by a quenched disorder. Obviously, the factor A is different in both cases. We use the same notation to stress the similar role played by this prefactor of M^d in both cases. Performing again a Gaussian integral of M^d over $\mathbf{r}-\mathbf{r}'$ we obtain

$$M^d(t)=\left(\frac{\sigma^2}{\pi\hbar^2}\right)^d\int d\mathbf{r}\sum_s C_s^2\left(\frac{2\pi\hbar^2}{A}\right)^{d/2} \times\exp\left[-\frac{2\sigma^2}{\hbar^2}(\bar{\mathbf{p}}_s-\mathbf{p}_0)^2\right]. \tag{3.32}$$

Under the same assumptions as in Sec. II D, we are led to a result equivalent to that of Eq. (2.31):

$$M^d(t)\simeq\bar{A}e^{-\lambda t}, \tag{3.33}$$

with $\bar{A}=[\sigma m_0/(A^{1/2}t)]^d$. Therefore, for long times the diagonal part of the Loschmidt echo decays with a rate given by the classical Lyapunov exponent of the system,

$$\lim_{t\to\infty}\left(-\frac{1}{t}\ln[M^d(t)]\right)=\lambda. \tag{3.34}$$

Of course this limit actually implies a time $t\gg 1/\lambda$, but still lower than the time at which either localization or finite-size effects appears. In the following section we will study the competition between the diagonal and nondiagonal contributions.

F. Diagonal versus nondiagonal contributions

As we have previously shown, the Loschmidt echo is made out of nondiagonal and diagonal components, and within the time scales specified above, it can be written as

$$M(t)=\exp\left[-\frac{vt}{\tilde{\ell}}\right]+\bar{A}\exp[-\lambda t]. \tag{3.35}$$

Such a result holds for the perturbation Σ that we have discussed in this section [Eq. (3.11)], as well as for the quenched disorder of Sec. II [Eq. (2.14)]. The only difference lies in the form of the elastic mean free path $\tilde{\ell}$ and the prefactor $\bar{A}$, both of which are perturbation dependent. The decay of the LE will be controlled by the slowest of the two rates. A weak perturbation implies $\tilde{\ell}>v/\lambda$ and a dominance of the nondiagonal term, while for sufficiently strong perturbations verifying $\tilde{\ell}<v/\lambda$ (but weak enough in order not to modify appreciably the classical trajectories), the diagonal term (governed by the Lyapunov exponent) sets the decay of the LE. This perturbation-independent behavior, predicted in Ref. 18 has been observed in numerical simulations done on a number of systems.[20–35] In Ref. 22 the regime of dominance of the nondiagonal (diagonal) component has been interpreted and referred to as a Fermi golden rule (Lyapunov) regime, and we will use both terminologies in the discussions that follow.

From the previous discussion it is clear that the Lyapunov regime can only be observed beyond a critical value of the perturbation. The condition stated above for the strength of the perturbation, along with Eq. (3.23), yields for the model discussed in this section a critical value of the perturbation parameter α beyond which the Lyapunov regime is obtained:

$$\alpha_c=\frac{2\hbar}{m_0}\sqrt{\frac{\lambda}{v^3\ell}}. \tag{3.36}$$

We will discuss in Sec. IV the physical consequences of the above critical value and its dependence on various physical parameters.

IV. UNIVERSALITY OF THE LYAPUNOV REGIME

A. Correspondence between semiclassical and numerical calculations

The semiclassical results obtained in the previous sections are valid in the small-wavelength limit, and rely on various uncontrolled approximations. It is then important to perform numerical calculations for various model systems in order to compare against the semiclassical predictions, and to explore parameter regimes inaccessible to the theory. In this section we use the same numerical method of Ref. 21 (described in detail in Appendix B) to study the Lorentz gas with the mass tensor perturbation introduced in Sec. III. We extend previ-

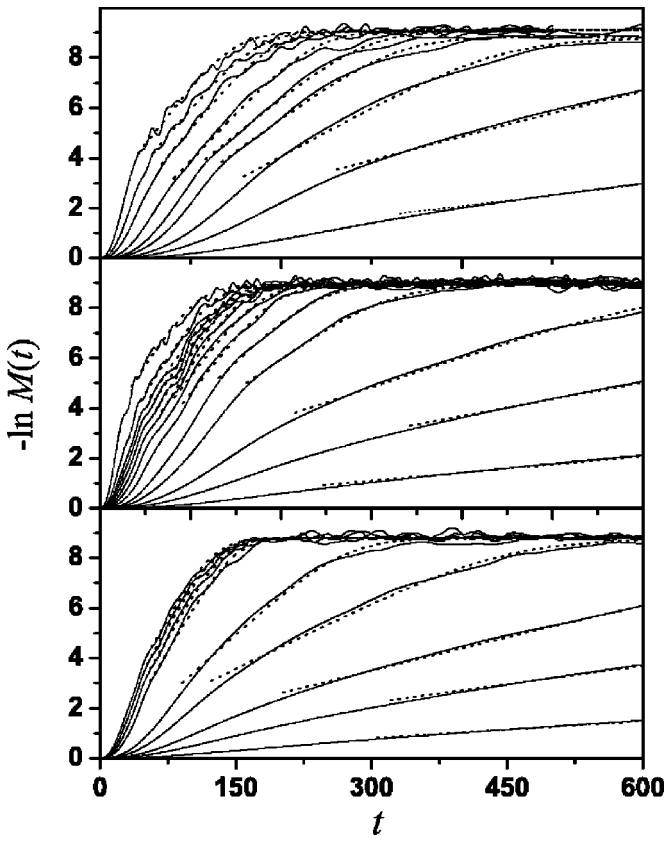

FIG. 3. Time decay of the Loschmidt echo $M(t)$ for different values of the perturbation strength α and concentration of impurities c. Top panel: $c=0.157$ and $\alpha=0.004$, 0.007, 0.01, 0.015, 0.02, 0.03, 0.05, 0.07, 0.1 (from top to bottom). Middle panel: $c=0.195$ and $\alpha=0.004$, 0.007, 0.01, 0.015, 0.02, 0.03, 0.04, 0.05, 0.06, 0.07, 0.08, 0.1, 0.15. Lower panel: $c=0.289$ and $\alpha=0.004$, 0.007, 0.01, 0.015, 0.02, 0.03, 0.04, 0.05, 0.06, 0.07. The time is measured in units of $\hbar/V$, where V is the hopping term of the tight-binding model (see Appendix B). The dashed lines represent the best fits to the decay, as described in the text.

ously known results in order to sustain the discussion on the universality of the Lyapunov regime. We will first focus on the behavior of the ensemble-averaged Loschmidt echo, followed by a thorough discussion of individual behavior and the averaging procedure.

We typically worked with disks of radius $R=20a$, and with a de Broglie wavelength $\lambda_B=2\pi/k=16/3a$. Here, a is the irrelevant lattice unit of our tight-binding model, which is decreased until the results only depend on the relation between physical parameters. The smallest system size allowing us to observe the exponential decay of $M(t)$ over a large interval was found to be $L=200a$ which leads to a Hilbert space with 4×10^4 states. We calculated $M(t)$ for different strengths of the perturbation α and concentration of disks c. In Fig. 3 we show our results for $c=0.157$, 0.195, and 0.289, and different values of α.

The time evolution of the LE presents various regimes. First, for very short times, $M(t)$ exhibits a Gaussian decay, $M(t)=\exp[-b\alpha^2t^2]$, where b is a parameter that depends on the initial state, the dynamics of $\mathcal{H}_0$, and the form of the perturbation Σ. This initial decay corresponds to the overlap of the perturbed and unperturbed wave packets whose centers separate linearly with time by the sole effect of the perturbation. This regime ends approximately at the typical time of the first collision.

Second, for intermediate times we find the region of interest for the semiclassical theory. In this time scale the LE decays exponentially with a characteristic time τ_ϕ. We reserve the symbol τ_ϕ for the decay rate, in view of its interpretation in terms of quantum decoherence (as we discuss in Sec. V). For small perturbations, τ_ϕ depends on α. We observe that for all concentrations there is a critical value α_c beyond which τ_ϕ is independent of the perturbation. Clearly, the initial perturbation-dependent Gaussian decay prevents the curves to be superimposed.

Finally, for very large times the LE saturates at a value M_∞ that depends on the system size L, but could also depend on the diffusion constant D. This regime is discussed in detail in the following sections. However, let us observe that in the crossover between the exponential decay and the long-time saturation there is a power-law decay with a perturbation-independent exponent. This is a manifestation of the underlying diffusive dynamics that leads to the isotropic state.

In order to compare our numerical results of $M(t)$ with the semiclassical predictions, we extract τ_ϕ by fitting $\ln M(t)$ to $\ln[A\exp(-t/\tau_\phi)+M_\infty]$. The dashed lines in Fig. 3 correspond to the best fits obtained with this procedure. The values of τ_ϕ for the different concentrations are shown as a function of the perturbation strength in Fig. 4. In agreement with our analytical results of the preceding section, we see that $1/\tau_\phi$ grows quadratically with the perturbation strength up to a critical value α_c, beyond which a plateau appears at the corresponding Lyapunov exponent. The dashed lines are the best fits to a quadratic behavior. The values obtained in this way agree with those predicted by the semiclassical theory [Eq. (3.23)] for the nondiagonal (FGR) term. The saturation values above α_c are well described by the corresponding Lyapunov exponents (solid lines), in agreement with the semiclassical prediction [Eq. (3.34)]. The very good quantitative agreement between the semiclassical and numerical calculations for the Lorentz gas (as well as in the case of other models[22,24,25]) strongly supports the generality of the saturation of τ_ϕ at a critical value of the perturbation strength.

The FGR exponent, which depends on $\mathcal{H}_0$ but not much on its chaoticity,[22,31] is given by the typical squared matrix element of Σ, and the density of connected final states $1/\Delta$. Hence, different $\mathcal{H}_0$ change the wave functions. That is why we observe that, for fixed perturbation strength α, the factor $v/\tilde{\ell}$ depends on the concentration of impurities of $\mathcal{H}_0$ (see inset of Fig. 4, where a log-log scale has been chosen in order to magnify the small perturbation region).

Notably, the dependence of $v/\tilde{\ell}$ with $\mathcal{H}_0$ leads to a counterintuitive effect (clearly observed in the inset of Fig. 4), namely, that the critical value needed for the saturation of $1/\tau_\phi$ is smaller for less chaotic systems (smaller λ). The reason for this is that in more dilute systems Σ is constant over larger straight pieces of trajectories (in between colli-

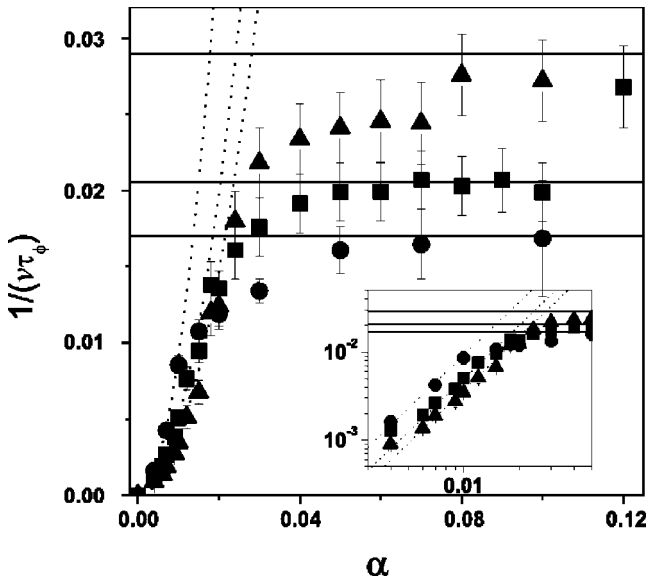

FIG. 4. Extracted values of the decay rate of the LE as a function of the perturbation strength for the three concentrations of Fig. 3. The rates are normalized to the group velocity of the initial wave packet ν, and we present $1/(\nu\tau_\phi)$ in units of a^{-1}; $c=0.157$ (circles), 0.195 (squares), and 0.289 (triangles). The solid lines are the corresponding classical Lyapunov exponents and the dashed lines are fits to the quadratic behavior predicted by Eq. (3.23). The predicted coefficients for the three concentrations are $72a^{-1}$, $55a^{-1}$, and $33a^{-1}$, while the obtained ones are $92a^{-1}$, $50a^{-1}$, and $37a^{-1}$, respectively. Inset: a log-log scale of the same data to show the quadratic increase of $1/\tau_\phi$ for small perturbations.

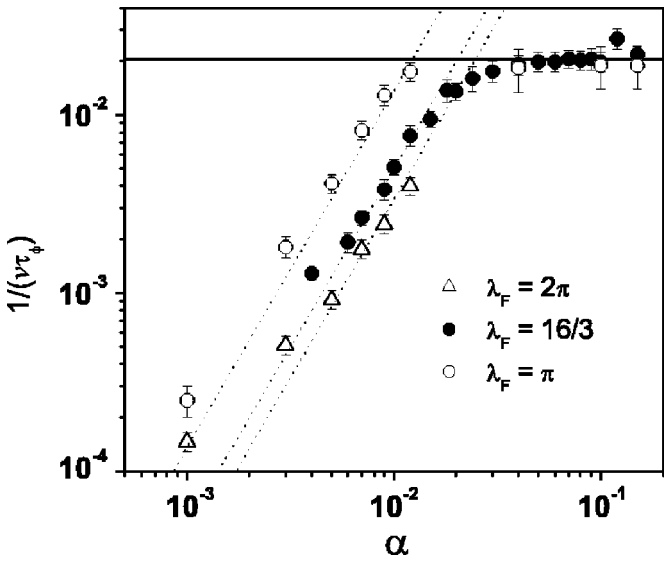

FIG. 5. Decay rates $1/\tau_\phi$ for different wavelengths λ_B of the initial wave packet for a concentration $c=0.195$ with the same units as in Fig 4. Solid line: classical Lyapunov exponent. Dashed line: the FGR quadratic behavior. Note that for decreasing λ_B the critical perturbation diminishes, implying a collapse of the Fermi golden rule regime.

sions), leading to a larger perturbation of the quantum phase and resulting in a stronger effective perturbation.

B. Universality of the Lyapunov regime in the semiclassical limit

Our semiclassical analysis yielded a critical value of the perturbation to enter in the Lyapunov regime [Eq. (3.36)], which vanishes in the semiclassical limit, $\alpha_c \to 0$ for $\hbar$ (or λ_B) $\to 0$, implying the collapse of the Fermi golden rule regime. This behavior is reproduced by our numerical calculations (Fig. 5). There, we decreased λ_B while keeping fixed the size σ of the initial wave packet. We note that, for a given value of the parameter α, the perturbation Σ [Eq. (3.11)] scales with the energy in a way that the underlying classical trajectories are always affected in the same way by the perturbation. The extracted crossover values of α_c are in quantitative agreement with Eq. (3.36), decreasing with λ_B in the interval that we were able to test.

Other choices of the perturbation Σ, such as the quenched disorder of Refs. 18 and 25, can be shown to give critical values that decrease with decreasing $\hbar$ as in Eq. (3.36), provided that the perturbation is scaled to the proper semiclassical limit. That is, for a fixed perturbation potential, we should take the limit of $\lambda_B \to 0$. As a result, if we keep $\hbar$ constant and decrease λ_B by increasing the particle energy, we should scale up the perturbation potential consistently (assuming that $\mathcal{H}_0$ generates the same dynamics at all energies).

We conclude that, in the semiclassical limit, any perturbation will be strong enough to put us in the Lyapunov regime, in consistency with the hypersensitivity expected for a classical system. It is then in this limit that the Lyapunov regime of the LE becomes universal, just as the case of classical chaos. This is not unexpected as in this limit the Ehrenfest time diverges and the correspondence principle should prevail.

We can draw a diagram separating FGR from Lyapunov regimes using the perturbation versus a scaling parameter determined by the particle energy (or inverse $\hbar$), as shown in Fig. 6. The gray shaded region corresponds to the Fermi golden rule regime and the clear one to the Lyapunov regime. The line that divides both phases is given by the critical perturbation, Eq. (3.36), which agrees with the numerical values of α_c extracted from Figs. 4 and 5 (black dots). The perturbative regime (PT, when the typical matrix element of Σ is smaller than the mean level spacing Δ) is sketched by the white dashed region of Fig. 6. This part of the diagram is only qualitative since the variables used in the figure are not the appropriate to describe the transition from this regime to the FGR. The transition value of the perturbation between FGR and PT regimes goes to zero in the semiclassical limit of $\lambda_B \to 0$ faster than α_c. Finally, the Lyapunov regime is bounded from above by an $\hbar$ independent critical value α_p (not shown in the figure due to the scale), marking the classical breakdown that we discuss below.

The interesting conceptual feature highlighted by Fig. 6 is the importance of the order in which we take the limits of Σ and λ_B going to zero. Two distinct results are obtained for the different order in which we can take this double limit. As depicted in the figure (with arrows representing the limits), $\lim_{\lambda_B \to 0}[\lim_{\Sigma \to 0}(1/\tau_\phi)] = 0$. On the other hand, taking the

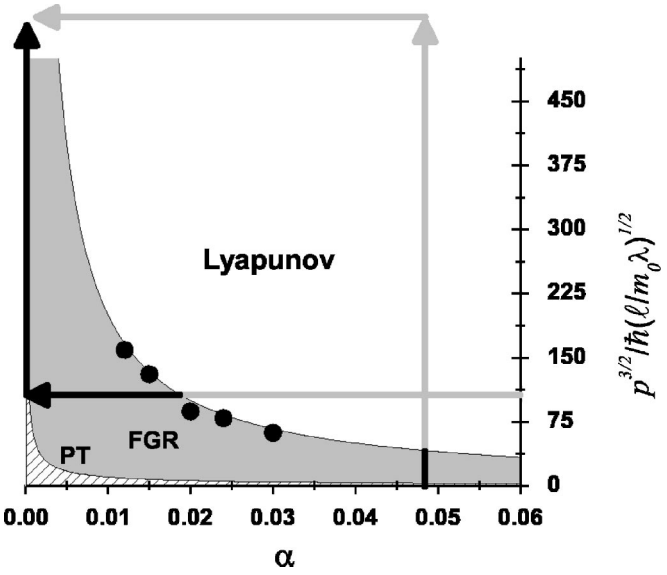

FIG. 6. Regime diagram for the Loschmidt echo as a function of the perturbation and the energy (or inverse $\hbar$). The gray area is the FGR regime with an α-dependent τ_ϕ, while the clear one is the Lyapunov regime with $\tau_\phi=\lambda^{-1}$. The line that divides both regimes is Eq. (3.36). The dots are the numerical values obtained from Figs. 4 and 5. The clear dashed region corresponds to typical parameters where perturbation theory applies. The arrows schematize the possible ordering of the double limit of the perturbation and the wavelength going to zero. Notice that the former ordering yields a vanishing τ_ϕ, while the latter one yields λ since we remain in the Lyapunov regime. For a strong enough perturbation (independent of $\hbar$ and out of scale in this figure) there is a breakdown of the Lyapunov regime.

inverse (more physical) ordering $\lim_{\Sigma\to 0}[\lim_{\lambda_B\to 0}(1/\tau_\phi)]=\lambda$ the semiclassical result is obtained. The resulting ''phase diagram'' representation for the different regimes of the LE is useful to illustrate that most often one is working in the region corresponding to the Lyapunov behavior.

Our semiclassical theory clearly fails when the perturbation is strong enough (or the times long enough) to appreciably modify the classical trajectories. This would give an upper limit (in perturbation strength) for the results of Sec. III. A more stringent limitation comes from the finite value of $\hbar$, due to the limitations of the diagonal approximations and linear expansions of the action that we have relied on. In other systems, such as the quenched disorder in a smooth stadium,[25] the upper critical value of the perturbation (for exiting the Lyapunov regime) can be related to the transport mean free path of the perturbation $\tilde{\ell}_{\rm tr}$, which is defined as the length scale over which the classical trajectories are affected by the disorder.[46]

We can obtain in our system an estimate of $\tilde{\ell}_{\rm tr}$ by considering the effect of the perturbation on a single scattering event. The difference $\delta\theta$ between the perturbed and unperturbed exit angles after the collision can be obtained using Eqs. (3.13), which results in

$$\delta\theta\sim 4n_x n_y\left(\frac{\mathbf{v}\cdot\mathbf{n}}{v}\right)^2\alpha, \tag{4.1}$$

where $\mathbf{v}$ is the initial velocity of the particle and $\mathbf{n}$ is the normal to the surface.

Assuming that the motion of the particle is not affected by chaos (nondispersive collisions), one can do a random-walk approach and estimate the mean-square distance after a time τ_{tr} from the fluctuations of the angle in Eq. (4.1). We estimate the transport mean free time as that at which the fluctuations are of the order of R, and obtain

$$\tilde{\ell}_{\rm tr}\simeq\frac{4R^2}{3\alpha^2\ell}, \tag{4.2}$$

assuming a uniform probability for the angle of the velocity as before. Equation (4.2) is used to get the upper bound perturbation $\alpha_{\rm p}$ for the end of the Lyapunov plateau,

$$\alpha_{\rm p}=\sqrt{\frac{4\lambda R^2}{3\ell v}}. \tag{4.3}$$

We obtain $\alpha_{\rm p}\simeq 0.23, 0.29$, and 0.43, respectively, for increasing magnitude of the three concentrations shown in Fig. 4. It is rather difficult to reach numerically these perturbations in our system, since the initial Gaussian decay drives $M(t)$ very quickly towards its saturation value, preventing the observation of an exponential regime. Despite this difficulty, we observe in Fig. 4 that the Lyapunov regime plateau appears to end for sufficiently strong perturbations. For the range we could explore the limiting values are in qualitative agreement with the estimation from Eq. (4.3).

C. Ehrenfest time and thermodynamic limit

We studied in the preceding section the behavior of the Lyapunov regime in the semiclassical limit $\hbar\to 0$; let us now turn our attention to the consequences of having a finite value of $\hbar$. In this case, one expects the propagation of a quantum wave packet to be described by the classical equations of motion up to the Ehrenfest time t_E, after which the quantum-classical correspondence breaks down.[37] Typically, t_E is the time when interference effects become relevant, and in a classically chaotic system it typically scales as $\ln[\hbar]$.

In other systems where the Lyapunov regime of the LE has been observed, such as chaotic maps or kicked systems, t_E coincides with the saturation time $t_s=1/\lambda\ \ln[N]$. This is because in these systems the number of states N plays the role of an effective Planck's constant $\hbar_{\rm eff}=1/N$. Therefore, when in these systems the LE is governed by a classical quantity, the whole range of interest occurs before the Ehrenfest time. It is then impossible from that evidence to conclude if the independence of the decay rate on the perturbation strength is a trivial consequence of the quantum-classical correspondence before t_E, a possibility that is supported by the fact that this is the regime of validity of the semiclassical theory.

In the Lorentz gas, however, we can differentiate between the time scales t_s and t_E by appropriately controlling the parameters. This is a property not shared by finite systems, but robust for extended ones such as the Lorentz gas. This does not imply an unbounded exponential decay of the LE, as discussed below. The saturation time is given by

$$t_s \simeq \frac{2}{\lambda} \ln\left[\frac{L}{\sigma}\right], \tag{4.4}$$

while the Ehrenfest time, defined as the time it takes for a minimal wave packet of wavelength λ_B to spread over a distance of the order of R,[54] is given by

$$t_E \simeq \frac{1}{\lambda} \ln\left[\frac{2R}{\lambda_B}\right]. \tag{4.5}$$

Our numerical calculations support these approximations.

The dependence of the saturation value M_∞ as a function of the inverse system size $1/L^2$ was previously studied in Ref. 16. Supposing that for long times the chaotic nature of the system will equally mix the $\tilde{N}=(L/\sigma)^2$ levels appreciably represented in the initial state with random phases ϕ_j, we write

$$M_\infty = \frac{1}{\tilde{N}^2} \left| \sum_j \exp[i(\phi_j - \phi_j')] \right|^2 = \frac{1}{\tilde{N}}. \tag{4.6}$$

We find numerically $M_\infty = (0.6 \pm 0.1)(\sigma/L)^2$ which confirms the prediction.

According to the above results, the Lyapunov regime shares the universality of its classical counterpart for arbitrarily large times in the thermodynamic limit of the size of the system going to infinity. However, this occurs only for times smaller than the critical time where the saturation value coincides with the space explored by the particle. In other words, for infinite unbounded systems there could be a breakdown of the exponential decay of the LE when the wave function expands over the ''available'' (time dependent) Hilbert space, which in the case of the Lorentz gas would follow a diffusive law. Therefore, the exponential decay of the quantum yields to a power law associated with the Pollicot-Ruelle diffusive modes when $\exp(-\lambda t) \approx \sigma^2/r^2(t)$, where $r^2(t)=2dDt$. In the case of the Lorentz gas, this time t_s^* is independent of the box size L and is approximately the solution of

$$t_s^* \sim \frac{1}{\lambda} \ln \frac{\ell v t_s^*}{\sigma^2}. \tag{4.7}$$

While the precise determination of Eq. (4.7) is beyond the reach of our computational resources, for times shorter than t_s^*, the expanding range of the exponential with L for times larger than t_E, where the correspondence principle does not prevail, was exemplified in Fig. 3 of Ref. 21. The survival of a classical signature of the quantum dynamics after the Ehrenfest time is due to a more complex effect, namely, the environment which, through the perturbation, randomizes the phase of the wave function and washes out terms of quantum nature. We will discuss this process and its relation to decoherence in detail in the following section.

D. Individual versus ensemble-average behavior

In order to make analytical progress, in our semiclassical calculations as well as in those of Ref. 18, an ensemble average was introduced (over realizations of the quenched disordered perturbation or over initial conditions). This approximation raises the question of whether the exponential decay of $M(t)$ is already present in individual realizations or, on the contrary, the averaging procedure is a crucial ingredient in obtaining a relaxation rate independent of the perturbation.[60]

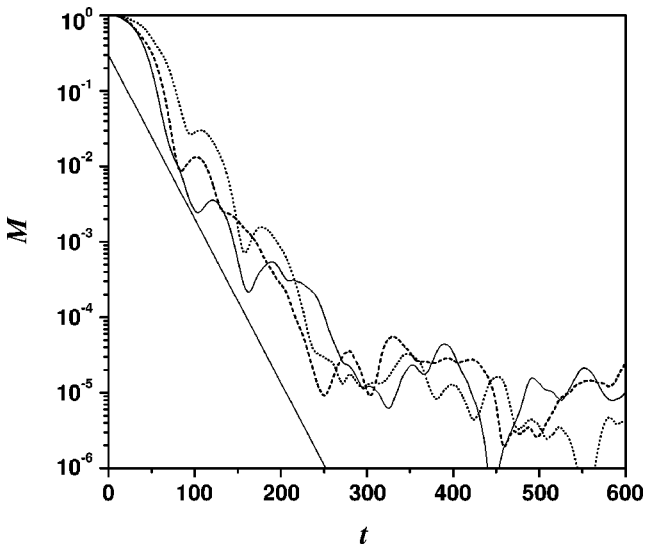

FIG. 7. $M(t)$ for three different single initial conditions of the wave packet. All the curves oscillate around the straight line, which is the decay corresponding to the Lyapunov exponent.

As it was discussed in Secs. II and III, for trajectories longer than the correlation length ξ of the perturbation, the contributions to ΔS from segments separated by more than ξ are uncorrelated. This leads us to consider that the decay observed for a single initial condition will be equivalent to that of the average. In this section we test this idea numerically.

For large enough systems presenting a large saturation time, we expect $M(t)$ to fluctuate around an exponential decay. This expectation is clearly supported by our numerical results shown in Fig. 7, where we present $M(t)$ for three different initial conditions in a system with $L=800a$ and fixed $\alpha=0.024$. An exponential decay with the semiclassical exponent is shown for comparison (thin solid line).

In order to obtain the exponent of the decay with a good precision, we can calculate $M(t)$ for a single initial condition in a large enough system. Alternatively, our results show that it is correct to obtain the exponent through an ensemble average to reduce the size of the fluctuations. However, as the former method is computationally much more expensive, we resort to the latter.

This situation is analogous to the classical case where one obtains the Lyapunov exponent from a single trajectory taking the limit of the initial distance going to zero and the time going to infinity, or else resorts to more practical methods such as the algorithm of Benettin *et al.* that averages distances over short evolutions.

Notice that in the Lorentz gas the average over initial conditions and the average over realizations of the impurities positions are equivalent. In all cases we have implemented

the last choice, for its computational convenience, and we use the term initial conditions to refer also to realizations of $\mathcal{H}_0$.

In particular, for our calculations, the average is constrained to those systems where the classical trajectory of the wave packet collides with at least one of the scatterers. This restriction helps avoid those configurations where a ''corridor'' exists, in which case $M(t)$ presents a power-law decay possibly related to the behavior found in integrable systems.[31,32]

The averaging of quantities that fluctuate around an exponential decay is a delicate matter, since different procedures can lead to quite different results. In particular, for the LE it has been noted that averaging $M(t)$ over initial conditions can result in an exponential decay different than the one of a single initial condition.[23,60] Given the exponential dependence of $M(t)$ in λ, the phase-space fluctuations of the Lyapunov exponent will induce a difference between the average $\ln M(t)$ and that of $M(t)$. The former procedure is more appropriate in order to have averages of the order of the typical values. On the other hand, if the fluctuations of the exponent are small, both procedures give similar results. This is the situation we found in our model system.

For the Lorentz gas we calculated $\langle M(t)\rangle$ and $\langle \ln M(t)\rangle$ and extracted the decay rates of the exponential regime using the fit described in Sec. IV A. We observe that the difference of the rates obtained through both averaging procedures is smaller than the statistical error. However, the observed relative error in the time regime of interest is smaller when averaging the logarithm of $M(t)$. Also, the difference in the actual values of $\langle M(t)\rangle$ and $\langle \ln M(t)\rangle$ is constant throughout the decay, the latter being larger.

V. ANALYSIS OF DECOHERENCE THROUGH THE LOSCHMIDT ECHO

A. Classical evolution of the Wigner function

As discussed in the Introduction, the Loschmidt echo can be obtained from the evolution of the Wigner function with the perturbed and unperturbed Hamiltonians [Eq. (1.2)]. Such a framework is particularly useful in the study of decoherence, as the Wigner function is a privileged tool to understand the connection between quantum and classical dynamics.[35,45]

The evolution of the wave functions in terms of the propagators [Eq. (2.2)] can be used to express the time dependence of the Wigner function as

$$W(\mathbf{r},\mathbf{p};t)=\frac{1}{(2\pi\hbar)^d}\int d\,\delta\mathbf{r}\int d\overline{\mathbf{r}}\int d\,\delta\overline{\mathbf{r}}\int d\overline{\mathbf{p}}W(\overline{\mathbf{r},\mathbf{p}};0)\times\exp\left[\frac{i}{\hbar}(\mathbf{p}\cdot\delta\mathbf{r}-\overline{\mathbf{p}}\cdot\delta\overline{\mathbf{r}})\right]K\left(\mathbf{r}-\frac{\delta\mathbf{r}}{2},\overline{\mathbf{r}}-\frac{\delta\overline{\mathbf{r}}}{2};t\right)\times K^*\left(\mathbf{r}+\frac{\delta\mathbf{r}}{2},\overline{\mathbf{r}}+\frac{\delta\overline{\mathbf{r}}}{2};t\right),\tag{5.1}$$

where $W(\overline{\mathbf{r},\mathbf{p}};0)$ is the initial Wigner function. The semiclassical expansion of the propagators [Eq. (2.4)] leads to the propagation of the Wigner function by ''chords,''[61–63] where pairs of trajectories $(s,\tilde{s})$ traveling from $(\overline{\mathbf{r}}-\delta\overline{\mathbf{r}}/2,\overline{\mathbf{r}}+\delta\overline{\mathbf{r}}/2)$ to $(\mathbf{r}-\delta\mathbf{r}/2,\mathbf{r}+\delta\mathbf{r}/2)$ have to be considered. In the leading order in $\hbar$ we can approximate the above propagators by sums over trajectories going from $\overline{\mathbf{r}}$ to $\mathbf{r}$, and the semiclassical evolution of the Wigner function is given by

$$W(\mathbf{r},\mathbf{p};t)=(2\pi\hbar)^d\int d\overline{\mathbf{r}}\int d\overline{\mathbf{p}}W(\overline{\mathbf{r},\mathbf{p}};0)\sum_{s,s'}\delta\left(\overline{\mathbf{p}}-\frac{\overline{\mathbf{p}}_s+\overline{\mathbf{p}}_{s'}}{2}\right)\times\delta\left(\mathbf{p}-\frac{\mathbf{p}_s+\mathbf{p}_{s'}}{2}\right)K_s(\mathbf{r},\overline{\mathbf{r}};t)K^*_{s'}(\mathbf{r},\overline{\mathbf{r}};t),\tag{5.2}$$

where $\overline{\mathbf{p}}_s$ $(\mathbf{p}_s)$ and $\overline{\mathbf{p}}_{s'}$ $(\mathbf{p}_{s'})$ are the initial (final) momenta of the trajectories s and s', respectively. The dominant contribution arises from the diagonal term $s=s'$

$$W_c(\mathbf{r},\mathbf{p},t)=\int d\overline{\mathbf{r}}\sum_{s(\mathbf{r},\mathbf{r},t)}C_s\delta(\mathbf{p}-\mathbf{p}_s)W(\overline{\mathbf{r},\mathbf{p}_s};0).\tag{5.3}$$

Using the fact that C_s is the Jacobian of the transformation from $\overline{\mathbf{r}}$ to $\mathbf{p}_s$, we have

$$W_c(\mathbf{r},\mathbf{p};t)=\int d\mathbf{p}_s\,\delta(\mathbf{p}-\mathbf{p}_s)W(\overline{\mathbf{r},\mathbf{p}_s};0),\tag{5.4}$$

where the trajectories considered now are those that arrive to $\mathbf{r}$ with momentum $\mathbf{p}$. We note that $(\overline{\mathbf{r},\mathbf{p}})$ is the preimage of $(\mathbf{r},\mathbf{p})$ by the equations of motion acting on a time t. That is, $(\mathbf{r},\mathbf{p})=X_t(\overline{\mathbf{r},\mathbf{p}})$. The momentum integral is trivial, and we obtain the obvious result

$$W_c(\mathbf{r},\mathbf{p};t)=W(\overline{\mathbf{r},\mathbf{p}};0),\tag{5.5}$$

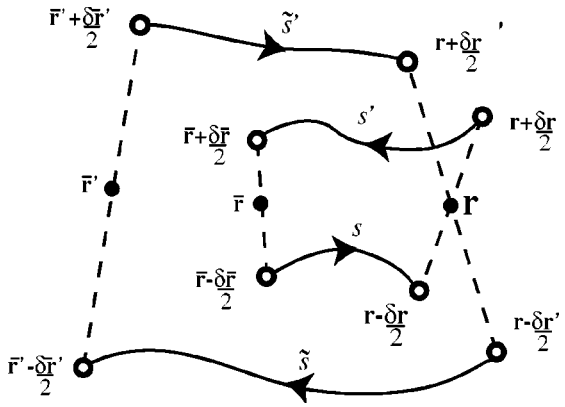

FIG. 8. Four classical trajectories used to compute semiclassically the Loschmidt echo through the evolution of two Wigner functions associated with different Hamiltonians.

with $(\overline{\mathbf{r}},\overline{\mathbf{p}})=X_t^{-1}(\mathbf{r},\mathbf{p})$. Since X_t conserves the volume in phase space, at the classical level the Wigner function evolves by simply following the classical flow.

B. Fine structure of the Wigner function and nonclassical contributions to the Loschmidt echo

As indicated in Eq. (1.2), the Loschmidt echo is given by the phase-space trace of two Wigner functions associated with slightly different Hamiltonians ($\mathcal{H}_0$ and $\mathcal{H}_0+\Sigma$). In order to facilitate the discussion, we introduce the density (or partial trace) f_Σ writing the LE as

$$M(t)=\int d\mathbf{r} f_\Sigma(\mathbf{r},t) \tag{5.6}$$

with

$$\begin{aligned} f_\Sigma(\mathbf{r},t)=\frac{1}{(2\pi\hbar)^d}\int d\mathbf{p}\int d\delta\mathbf{r}\int d\overline{\mathbf{r}}\int d\delta\overline{\mathbf{r}}\int d\overline{\mathbf{p}}\int d\delta\mathbf{r}'\int d\overline{\mathbf{r}}'\int d\delta\overline{\mathbf{r}}'\int d\overline{\mathbf{p}}'\,W(\overline{\mathbf{r}},\overline{\mathbf{p}};0)\\ \times W^*(\overline{\mathbf{r}}',\overline{\mathbf{p}}';0)\exp\left[\frac{i}{\hbar}(\mathbf{p}\cdot\delta\mathbf{r}-\overline{\mathbf{p}}\cdot\delta\overline{\mathbf{r}})\right]\exp\left[-\frac{i}{\hbar}(\mathbf{p}\cdot\delta\mathbf{r}'-\overline{\mathbf{p}}'\cdot\delta\overline{\mathbf{r}}')\right]\\ \times K\left(\mathbf{r}-\frac{\delta\mathbf{r}}{2},\overline{\mathbf{r}}-\frac{\delta\overline{\mathbf{r}}}{2};t\right)K^*\left(\mathbf{r}+\frac{\delta\mathbf{r}}{2},\overline{\mathbf{r}}+\frac{\delta\overline{\mathbf{r}}}{2};t\right)\tilde{K}^*\left(\mathbf{r}-\frac{\delta\mathbf{r}'}{2},\overline{\mathbf{r}}'-\frac{\delta\overline{\mathbf{r}}'}{2};t\right)\tilde{K}\left(\mathbf{r}+\frac{\delta\mathbf{r}'}{2},\overline{\mathbf{r}}'+\frac{\delta\overline{\mathbf{r}}'}{2};t\right). \end{aligned} \tag{5.7}$$

K and $\tilde{K}$ represent the propagators associated with $\mathcal{H}_0$ and $\mathcal{H}_0+\Sigma$, respectively. The semiclassical evolution of f_Σ is given by sets of four trajectories, as illustrated in Fig. 8.

As we have consistently done in this work, we take Gaussian wave packet (of width σ) as initial state. Its associated Wigner function reads

$$W(\overline{\mathbf{r}},\overline{\mathbf{p}};0)=\frac{1}{(\pi\hbar)^d}\exp\left[-\frac{(\overline{\mathbf{r}}-\mathbf{r}_0)^2}{\sigma^2}-\frac{(\overline{\mathbf{p}}-\mathbf{p}_0)^2\sigma^2}{\hbar^2}\right]. \tag{5.8}$$

Assuming that Σ constitutes a small perturbation, after a few trivial integrations we obtain

$$\begin{aligned} f_\Sigma(\mathbf{r},t)=\frac{\sigma^2}{(2\pi^3\hbar^4)^{d/2}}\int d\delta\mathbf{r}\int d\overline{\mathbf{r}}\int d\delta\overline{\mathbf{r}}\int d\overline{\mathbf{p}}\int d\delta\overline{\mathbf{r}}'\int d\overline{\mathbf{p}}'\exp\left[\frac{i}{\hbar}(\overline{\mathbf{p}}'\cdot\delta\overline{\mathbf{r}}'-\overline{\mathbf{p}}\cdot\delta\overline{\mathbf{r}})\right]\exp\left[-\frac{2}{\sigma^2}(\overline{\mathbf{r}}-\mathbf{r}_0)^2\right]\\ \times\exp\left[-\frac{\sigma^2}{\hbar^2}[(\overline{\mathbf{p}}-\mathbf{p}_0)^2+(\overline{\mathbf{p}}'-\mathbf{p}_0)^2]\right]\sum_{s,s'}\sum_{\tilde{s},\tilde{s}'}\exp\left[-\frac{\mathcal{P}^2\sigma^2}{8\hbar^2}\right]K_s\left(\mathbf{r}-\frac{\delta\mathbf{r}}{2},\overline{\mathbf{r}}-\frac{\delta\overline{\mathbf{r}}}{2};t\right)K_{s'}^*\left(\mathbf{r}+\frac{\delta\mathbf{r}}{2},\overline{\mathbf{r}}+\frac{\delta\overline{\mathbf{r}}}{2};t\right)\\ \times K_{\tilde{s}}^*\left(\mathbf{r}-\frac{\delta\mathbf{r}}{2},\overline{\mathbf{r}}-\frac{\delta\overline{\mathbf{r}}'}{2};t\right)K_{\tilde{s}'}\left(\mathbf{r}+\frac{\delta\mathbf{r}}{2},\overline{\mathbf{r}}+\frac{\delta\overline{\mathbf{r}}'}{2};t\right), \end{aligned} \tag{5.9}$$

where we have defined

$$\mathcal{P}=\overline{\mathbf{p}}_s+\overline{\mathbf{p}}_{\tilde{s}}-\overline{\mathbf{p}}_{s'}-\overline{\mathbf{p}}_{\tilde{s}'}. \tag{5.10}$$

Now the trajectories s and $\tilde{s}$ (s' and $\tilde{s}'$) arrive to the same final point $\overline{\mathbf{r}}-\delta\overline{\mathbf{r}}/2$ ($\mathbf{r}+\delta\mathbf{r}/2$). Since the initial wave packet is concentrated around $\mathbf{r}_0$, we can further simplify and work with trajectories s and $\tilde{s}$ (s' and $\tilde{s}'$) that have the same extreme points. Therefore, we have

$$\begin{aligned} f_\Sigma(\mathbf{r},t)=\frac{\sigma^2}{(2\pi^3\hbar^4)^{d/2}}\int d\delta\mathbf{r}\int d\overline{\mathbf{r}}\int d\delta\overline{\mathbf{r}}\exp\left[-\frac{2}{\sigma^2}(\overline{\mathbf{r}}-\mathbf{r}_0)^2\right]\sum_{s,s'}\sum_{\tilde{s},\tilde{s}'}\exp\left[-\frac{\mathcal{P}^2\sigma^2}{8\hbar^2}-\frac{2\sigma^2}{\hbar^2}\left(\frac{\mathcal{R}}{4}-\mathbf{p}_0\right)^2-\frac{\delta\overline{r}^2}{2\sigma^2}\right]\\ \times K_s\left(\mathbf{r}-\frac{\delta\mathbf{r}}{2},\overline{\mathbf{r}}-\frac{\delta\overline{\mathbf{r}}}{2};t\right)K_{s'}^*\left(\mathbf{r}+\frac{\delta\mathbf{r}}{2},\overline{\mathbf{r}}+\frac{\delta\overline{\mathbf{r}}}{2};t\right)K_{\tilde{s}}^*\left(\mathbf{r}-\frac{\delta\mathbf{r}}{2},\overline{\mathbf{r}}-\frac{\delta\overline{\mathbf{r}}}{2};t\right)K_{\tilde{s}'}\left(\mathbf{r}+\frac{\delta\mathbf{r}}{2},\overline{\mathbf{r}}+\frac{\delta\overline{\mathbf{r}}}{2};t\right), \end{aligned} \tag{5.11}$$

with

$$\mathcal{R}=\overline{\mathbf{p}}_s+\overline{\mathbf{p}}_{\tilde{s}}+\overline{\mathbf{p}}_{s'}+\overline{\mathbf{p}}_{\tilde{s}'}. \tag{5.12}$$

By the same considerations as before, we can reduce all four trajectories to start at the center $\mathbf{r}_0$ of the initial wave packet (Fig. 9)

$$f_\Sigma(\mathbf{r},t)=(4\pi\sigma^2)^d\int d\,\delta\mathbf{r}\sum_{s,\tilde{s}}\sum_{s',\tilde{s}'}\exp\left[-\frac{(\mathcal{P}^2+\mathcal{S}^2+\mathcal{T}^2)\sigma^2}{8\hbar^2}\right]\exp\left[-\frac{2\sigma^2}{\hbar^2}\left(\frac{\mathcal{R}}{4}-\mathbf{p}_0\right)^2\right]$$
$$\times K_s\left(\mathbf{r}-\frac{\delta\mathbf{r}}{2},\mathbf{r}_0;t\right)K^*_{s'}\left(\mathbf{r}+\frac{\delta\mathbf{r}}{2},\mathbf{r}_0;t\right)K^*_{\tilde{s}}\left(\mathbf{r}-\frac{\delta\mathbf{r}}{2},\mathbf{r}_0;t\right)K_{\tilde{s}'}\left(\mathbf{r}+\frac{\delta\mathbf{r}}{2},\mathbf{r}_0;t\right), \tag{5.13}$$

with

$$\mathcal{S}=\overline{\mathbf{p}}_s-\overline{\mathbf{p}}_{\tilde{s}}+\overline{\mathbf{p}}_{s'}-\overline{\mathbf{p}}_{\tilde{s}'}, \tag{5.14a}$$

$$\mathcal{T}=\overline{\mathbf{p}}_s+\overline{\mathbf{p}}_{\tilde{s}}-\overline{\mathbf{p}}_{s'}-\overline{\mathbf{p}}_{\tilde{s}'}. \tag{5.14b}$$

Given that

$$\mathcal{P}^2+\mathcal{S}^2+\mathcal{T}^2=(\overline{\mathbf{p}}_s-\overline{\mathbf{p}}_{\tilde{s}})^2+(\overline{\mathbf{p}}_s-\overline{\mathbf{p}}_{s'})^2+(\overline{\mathbf{p}}_s-\overline{\mathbf{p}}_{\tilde{s}'})^2+(\overline{\mathbf{p}}_{\tilde{s}}-\overline{\mathbf{p}}_{s'})^2+(\overline{\mathbf{p}}_{\tilde{s}}-\overline{\mathbf{p}}_{\tilde{s}'})^2+(\overline{\mathbf{p}}_{s'}-\overline{\mathbf{p}}_{\tilde{s}'})^2, \tag{5.15}$$

and since the pairs of trajectories $(s,\tilde{s})$ and $(s',\tilde{s}')$ have the same extreme points, the dominant contribution to f_Σ will come from the terms with $s=\tilde{s}$ and $s'=\tilde{s}'$. Such an identification minimizes the oscillatory phases of the propagators, and corresponds to the first diagonal approximation of the calculation of Sec. II and Ref. 18. Within such an approximation we have

$$f_\Sigma(\mathbf{r},t)=\left(\frac{\sigma^2}{\pi\hbar^2}\right)^d\int d\,\delta\mathbf{r}\sum_{s,s'}C_sC_{s'}\exp\left[-\frac{(\overline{\mathbf{p}}_s-\overline{\mathbf{p}}_{s'})^2\sigma^2}{2\hbar^2}-\frac{2\sigma^2}{\hbar^2}\left(\frac{\overline{\mathbf{p}}_s+\overline{\mathbf{p}}_{s'}}{2}-\mathbf{p}_0\right)^2\right]$$
$$\times\exp\left\{\frac{i}{\hbar}\left[\Delta S_s\left(\mathbf{r}-\frac{\delta\mathbf{r}}{2},\mathbf{r}_0,t\right)-\Delta S_{s'}\left(\mathbf{r}+\frac{\delta\mathbf{r}}{2},\mathbf{r}_0,t\right)\right]\right\}. \tag{5.16}$$

As in Eq. (2.10), $\Delta S_{s,s'}$ is the extra contribution to the classical action that the trajectory $\tilde{s}$ ($\tilde{s}'$) acquires with respect to s (s') by effect of the perturbation Σ.

We have two different cases, depending on whether or not there are trajectories leaving from $\mathbf{r}_0$ with momentum close to $\mathbf{p}_0$ that arrive to the neighborhood of $\mathbf{r}$ after a time t. In the first case $\mathbf{r}$ is in the manifold that evolves classically from the initial wave packet (Fig. 10). Such a contribution is dominated by the terms where the trajectory s' remains close to its partner s. Calling f^d_Σ this diagonal component, we get

$$f^d_\Sigma(\mathbf{r},t)=\left(\frac{\sigma^2}{\pi\hbar^2}\right)^d\int d\,\delta\mathbf{r}\sum_{s,s'}C_s^2\exp\left[-\frac{2\sigma^2}{\hbar^2}(\overline{\mathbf{p}}_s-\mathbf{p}_0)^2\right]\exp\left\{\frac{i}{\hbar}\left[\Delta S_s\left(\mathbf{r}-\frac{\delta\mathbf{r}}{2},\mathbf{r}_0,t\right)-\Delta S_{s'}\left(\mathbf{r}+\frac{\delta\mathbf{r}}{2},\mathbf{r}_0,t\right)\right]\right\}. \tag{5.17}$$

Assuming, as in Sec. II and Ref. 18, that $\mathcal{H}_0$ stands for a chaotic system and that the perturbation Σ represents a quenched disorder, upon average we obtain

$$\left\langle\exp\left\{\frac{i}{\hbar}\left[\Delta S_s\left(\mathbf{r}-\frac{\delta\mathbf{r}}{2},\mathbf{r}_0,t\right)-\Delta S_{s'}\left(\mathbf{r}+\frac{\delta\mathbf{r}}{2},\mathbf{r}_0,t\right)\right]\right\}\right\rangle$$
$$=\exp\left[-\frac{1}{2\hbar^2}A\,\delta r^2\right], \tag{5.18}$$

where A is given by Eq. (2.30). We therefore have

$$f^d_\Sigma(\mathbf{r},t)=\left(\frac{2\sigma^4}{\pi\hbar^2A}\right)^{d/2}\sum_{s(\mathbf{r}_0,\mathbf{r},t)}C_s^2\exp\left[-\frac{2\sigma^2}{\hbar^2}(\overline{\mathbf{p}}_s-\mathbf{p}_0)^2\right], \tag{5.19}$$

and the corresponding contribution to the Loschmidt echo is

$$M^d(t)=\int d\mathbf{r}\;\; f^d_\Sigma(\mathbf{r},t)$$
$$=\left(\frac{2\sigma^4}{\pi\hbar^2A}\right)^{d/2}\int d\overline{\mathbf{p}}\;\; C\;\; \exp\left[-\frac{2\sigma^2}{\hbar^2}(\overline{\mathbf{p}}-\mathbf{p}_0)^2\right]. \tag{5.20}$$

As in Eqs. (2.9) and (2.23) we have used C as the Jacobian of the transformation from $\mathbf{r}$ to $\overline{\mathbf{p}}$. Now the dominant trajectories are those starting from $\mathbf{r}_0$ and momentum $\mathbf{p}_0$. We are then back to the case of the previously discussed [Eqs. (2.31) and (3.33)] diagonal contribution

$$M^d(t)\simeq\overline{A}e^{-\lambda t}, \tag{5.21}$$

where $C=(m/t)^de^{-\lambda t}$ is assumed and $\overline{A}=(m\sigma/A^{1/2}t)^d$. The decay rate of the diagonal contribution is set by the

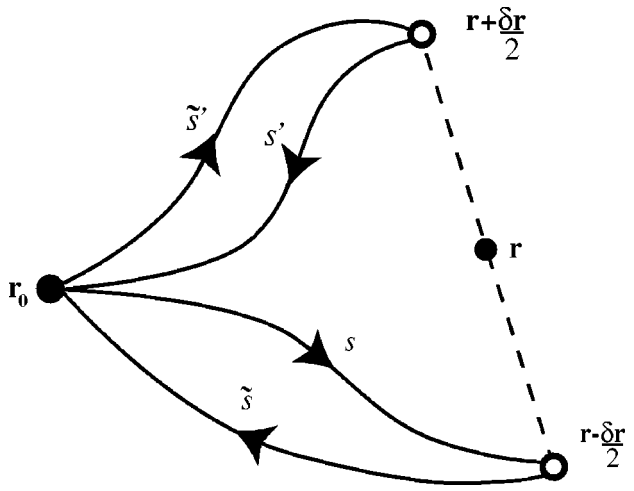

FIG. 9. For a fairly localized initial wave packet, the four classical trajectories contributing to the LE can be reduced to those starting at its center $\mathbf{r}_0$.

Lyapunov exponent λ, and therefore it is independent on the perturbation Σ.

The second possibility we have to consider is the case where there does not exist any trajectory leaving from $\mathbf{r}_0$ with momentum close to $\mathbf{p}_0$ that arrives to the neighborhood of $\mathbf{r}$ after a time t. It is a property of the Wigner function that in the region of phase space classically inaccessible by X_t the points $\mathbf{r}$ halfway between branches of the classically evolved distribution will yield the largest values of f_Σ (Fig. 11). The trajectories s and s' visit now different regions of the configuration space, therefore the impurity average can be done independently for each of them. As in Eq. (2.20), we have

$$\left\langle \exp\left[\frac{i}{\hbar}\Delta S_s\right]\right\rangle = \exp\left[-\frac{1}{2\hbar^2}\langle \Delta S_s^2\rangle\right] = \exp\left[-\frac{v_0 t}{2\tilde{\ell}}\right]. \tag{5.22}$$

Such an average only depends on the length $L=v_0 t$ of the trajectories. Thus, after average the nondiagonal term writes

$$f_\Sigma^{\mathrm{nd}}(\mathbf{r},t) = \left(\frac{\sigma^2}{\pi\hbar^2}\right)^d \exp\left[-\frac{v_0 t}{\tilde{\ell}}\right]\int d\,\delta\mathbf{r}\sum_{s,s'} C_s C_{s'} \times \exp\left[-\frac{\sigma^2}{\hbar^2}[(\overline{\mathbf{p}}_s-\mathbf{p}_0)^2+(\overline{\mathbf{p}}_{s'}-\mathbf{p}_0)^2]\right]. \tag{5.23}$$

The trajectory s (s') goes from the point $\mathbf{r}_0$ to $\mathbf{r}-\delta\mathbf{r}/2$ ($\mathbf{r}+\delta\mathbf{r}/2$). That is why the largest values of $f_\Sigma^{\mathrm{nd}}(\mathbf{r},t)$ are attained when $\mathbf{r}$ is in the middle of two branches of the classically evolved distribution. Other points $\mathbf{r}$ result in much smaller values of $f_\Sigma^{\mathrm{nd}}(\mathbf{r},t)$, since the classical trajectories that go between $\mathbf{r}_0$ and $\mathbf{r}\mp\delta\mathbf{r}/2$ require initial momenta $\overline{\mathbf{p}}_s$ ($\overline{\mathbf{p}}_{s'}$) very different from $\mathbf{p}_0$. Thus, exponentially suppressed contributions result.

The nondiagonal contribution to the Loschmidt echo can now be written as

$$M^{\mathrm{nd}}(t) = \int d\mathbf{r} f_\Sigma^{\mathrm{nd}}(\mathbf{r},t) = \left(\frac{\sigma^2}{\pi\hbar^2}\right)^d \exp\left[-\frac{v_0 t}{\tilde{\ell}}\right] \times \left|\int d\mathbf{r}\sum_s C_s \exp\left[-\frac{\sigma^2}{\hbar^2}[(\overline{\mathbf{p}}_s-\mathbf{p}_0)^2]\right]\right|^2 = \exp\left[-\frac{v_0 t}{\tilde{\ell}}\right]. \tag{5.24}$$

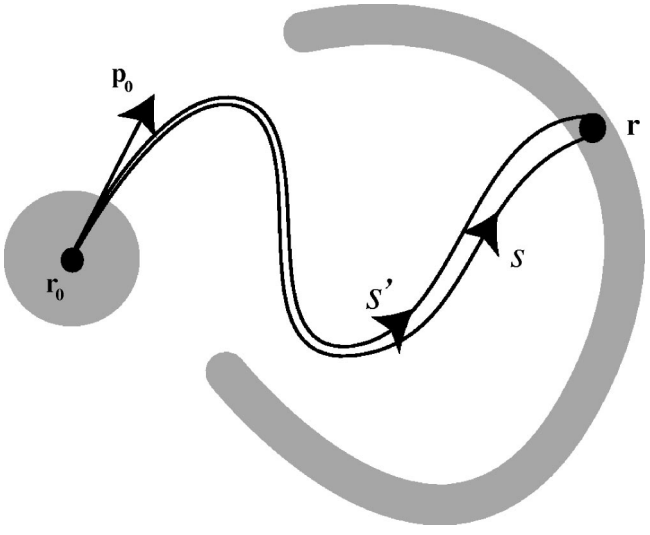

FIG. 10. Classical trajectories in the manifold that evolves classically from $\mathbf{r}_0$ to $\mathbf{r}$, representing the diagonal component of f_Σ. The action differences ΔS associated with the trajectories s and s' are correlated. The shaded regions depict the initial and final classical densities.

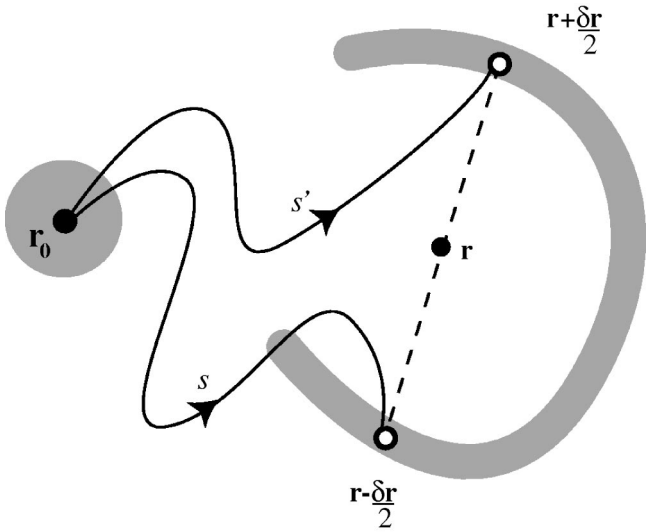

FIG. 11. Nondiagonal contribution to the LE given by trajectories departing from $\mathbf{r}_0$ and arriving to points equidistant from the point $\mathbf{r}$ where the Wigner function is evaluated. The action differences ΔS associated with both trajectories are uncorrelated.

As in Eqs. (2.23) and (3.22), we have made the change of variable from $\mathbf{r}$ to $\overline{\mathbf{p}}$, and accordingly, we have obtained the nondiagonal contribution to the LE.[18] As discussed before, such a contribution is a Fermi golden rule like.[22] In the limit of $\hbar \to 0$ our diagonal term, Eq. (5.21), obtained from the final points who follow the classical flow, dominates the LE, consistent with our findings of Sec. IV B.

C. Decoherence and emergence of classicality

Decoherence in a quantum system arises from its interaction with an external environment, over which the observers have neither information nor control.[64–66] The states more sensitive to decoherence are those with quantum superpositions (Schrödinger cat states), since they depend strongly on the information coded in the phase of the wave function, which is blurred by the interaction with the environment.

The studies of decoherence have traditionally considered one-dimensional systems, and often ignored the crucial role of its underlying classical dynamics.[67] On the other hand, it has been proposed[19] and later corroborated numerically[68] that for a classically chaotic system the entropy production rate (computed from its reduced density matrix) is given by the Lyapunov exponent. Moreover, as shown in Ref. 18 and thoroughly discussed in this work, the decay rate of the Loschmidt echo in a multidimensional classically chaotic system becomes independent of the strength of the perturbation that breaks the time reversal between two well-defined limits (and set by the Lyapunov exponent). The connection between decoherence and Loschmidt echo has been discussed in Refs. 18 and 69 and has induced us to denote as τ_ϕ the relaxation rate of the LE.

Decoherence is typically analyzed through the time decay of the off-diagonal matrix elements of the reduced density matrix (where the environmental degrees of freedom of the total density matrix of the system and its environment are traced out), while the wave-function superposition defining the LE can be cast as a trace of reduced density matrices or Wigner functions evolving with different Hamiltonians [Eq. (1.2)]. Zurek has recently proposed to consider the relevance of sub-Planck structure (in phase space) of the Wigner function for the study of quantum decoherence.[38] These structures appear when the wave function is made of a superposition of states, and they have large oscillations between large positive and negative values (called interference fringes for their similitude with a double-slit experience). It has then been proposed that the fringes substantially enhance the sensitivity of the quantum state to an external perturbation. A strong coupling with an environment suppresses the fringes, and the resulting Wigner function becomes positive everywhere and similar to the corresponding Liouville distribution of the equivalent classical system (with statistical mixtures instead of superpositions).[66] Jacquod and collaborators[43] have contested this approach, by demonstrating that the enhanced decay is described entirely by the classical Lyapunov exponent, and hence insensitive to the quantum interference that leads to the sub-Planck structures of the Wigner function.

Working with the superposition of two Wigner functions (as in the case of the echo) and with genuinely multidimensional classically chaotic systems allows us to give a consistent description of the connection between quantum decoherence and the Loschmidt echo the emergence of classical behavior. Here we remind the reader of our approach to decoherence: rather than introducing an environment in the quantum evolution and then tracing it out, we consider its effect on the system as a perturbation added to the Hamiltonian. We assume then that when the time reversal of the evolved wave function is performed, all uncontrolled degrees of freedom leave a mark as a unitary perturbation to the original Hamiltonian of the system. Of course, such a correspondence between environment and perturbation can be extremely cumbersome or even impossible to prove in a general case. In the particular case of an environment made of a bath of harmonic oscillators in the limit of high temperature, one can show that it is equivalent to having a random white noise perturbation in the Hamiltonian.[69] Although more research on this equivalence is desirable, we assume it is true at least in some general level. Therefore, we understand the LE as a measure of decoherence, and the results of the preceding section will be interpreted from the known behavior of the Wigner function in open systems.

From the semiclassical evolution of the Wigner function we were able to identify the nondiagonal component M^{nd} as the contribution to the LE given by the values of the Wigner function between the branches of the classically evolved initial distribution (Fig. 11). In this region both of the Wigner functions contributing to Eq. (1.2) are highly oscillating, and quite different from each other. The overlap, which is perfect for zero coupling (ensuring the unitarity requirement), is rapidly suppressed with increasing perturbation strength. As discussed earlier in the text (see also Refs. 18 and 22), when M^{nd} is the dominant contribution to M, we are in the Fermi golden rule regime. We have seen that this weak perturbation regime collapses as $\hbar \to 0$ [Eqs. (2.32) and (3.36)].

Beyond a critical perturbation, when the overlap coming from the oscillating part of the Wigner functions is suppressed, the diagonal component M^d takes over as the dominant contribution to the LE. It is given by the values of the Wigner function on the regions of phase space that result from the classical evolution of the initial distribution. This is the Lyapunov regime, where the decay rate of $M(t)$ is given by λ. Notice that this behavior is still of quantum origin, as we are comparing the increase of the actions of nearby trajectories by the effect of a small perturbation, assuming that the classical dynamics is unchanged. The behavior in the Lyapunov regime does not simply follow from the classical fidelity, where the change in the classical trajectories is taken into account, and the finite resolution with which we follow them plays a major role. The upper value of the perturbation strength for observing the Lyapunov regime is a classical one, i.e., $\hbar$ independent [$\ell_{\mathrm{tr}} \simeq L$ in Sec. II D and Eq. (4.3)].

For stronger perturbations (see discussions in Secs. II D and IV B) the classical trajectories are affected and the decay rate of the LE is again perturbation dependent. The Wigner function approach to the LE also helps us to develop our intuition about the quantum to classical transition. The

Lyapunov regime is the correct classical limit of a chaotic system weakly coupled to an external environment.

VI. CONCLUSIONS

In this work we have studied the decay of the Loschmidt echo in classically chaotic systems and presented evidence for the universality of the Lyapunov regime, where the relaxation rate becomes independent of the perturbation, and given by the Lyapunov exponent of the classical system. Using analytical and numerical calculations we have determined the range (in perturbation strength) of the Lyapunov regime, its robustness with respect to the classical limit, the form of the perturbation, the initial state, and the average conditions.

We presented semiclassical calculations in two different Hamiltonian systems: a classically chaotic billiard perturbed by quenched disorder and a Lorentz gas where the perturbation is given by an anisotropy of the mass tensor. In the latter model, the numerical simulations were found in good agreement with the analytical calculations, and showed that the Lyapunov decay extends well beyond the Ehrenfest time (where the quantum-classical correspondence is no longer expected to hold).

We remark that both our examples included some kind of disorder, rather in the perturbation or in the Hamiltonian. This is not crucial for the observation of the Lyapunov regime, as shown by numerical experiments in the Bunimovich stadium[24] and in the many maps studied. This independence from disorder can be related to the chaoticity of the Hamiltonian which randomizes the actions along a particular trajectory after a certain typical distance. However, the mentioned systems are bounded and therefore cannot rule out the relevance of disorder in the Lyapunov decay after the Ehrenfest time. Clarifying the role of disorder in this regime and in systems with weak or nonexistent chaos is certainly an interesting problem for future research.

Using a Wigner function representation, we have been able to present an alternative interpretation of the two contributions to the Loschmidt echo. The nondiagonal (Fermi golden rule) regime obtained for weak perturbation was shown to arise from the destruction of coherence between nonlocal superpositions, thus suppressing the nonclassical part of the distribution. In contrast, the diagonal (Lyapunov) regime obtained for stronger perturbation or more classical systems was shown to be given by the classical part of the evolved initial distribution. Thus, the Lyapunov regime is associated with the classical evolution (even though is of quantum origin), while the Fermi golden rule has a purely quantum nature. In this way, the persistence of the Lyapunov regime after Ehrenfest time is understood as the emergence of classical behavior due to the fast dephasing of the purely quantum terms. This is in consistency with the understanding of the quantum-classical transition in quantum systems coupled to an environment driven by the decoherence.[65]

The existence and universality of an environment-independent regime and its consequence in the phase-space behavior of the Wigner function provide a highlight on the connection between the Loschmidt echo and quantum decoherence. Such a connection, as well as the experiments testing the universal behavior, are promising subjects for future research.

The universal behavior of the Loschmidt echo requires an underlying classically chaotic system, such as the ones we have considered in this work. Hamiltonian systems with regular dynamics have been shown to exhibit nonuniversal behavior. Power laws[31] as well as Gaussian[32] behavior have been reported for the decay of the Loschmidt echo, depending on the form of the perturbation. This behavior is apparently quite different from the one we obtain for chaotic systems, and therefore we see that the Loschmidt echo constitutes a relevant concept in the study of quantum chaos.[13] Such a connection clearly deserves further studies. The Loschmidt echo in the Lorentz gas has been recently calculated for short times,[70] and a rate given by twice the Lyapunov exponent has been proposed. It would be interesting to investigate if the difference in time scales is responsible for the departure from our results.

ACKNOWLEDGMENTS

The authors would like to thank G. Benenti, Ph. Jacquod, P. R. Levstein, L. F. Foá Torres, and F. Toscano for fruitful discussions. We are grateful to G.-L. Ingold and G. Weick for their careful reading of the manuscript and valuable suggestions. H.M.P. was affiliated to CONICET. This work received financial support from CONICET, ANPCyT, SeCyT-UNC, Fundación Antorchas, the Institut universitaire de France, and the French-Argentinian program ECOS-Sud.

APPENDIX A: CLASSICAL DYNAMICS WITH AN ANISOTROPIC MASS TENSOR

Let us assume a particle in a free space with mass tensor $\vec{m}$ surrounded by an infinite potential surface (hard wall). Suppose that the particle departs from a point $\mathbf{r}_0$ at time t_0 and arrives to a final point $\mathbf{r}$ at time t. We must calculate the time t_c and position $\mathbf{r}_c$ along the surface at which the particle collides. The action along the trajectory is

$$S=\frac{(\mathbf{r}_c-\mathbf{r}_0)\vec{m}(\mathbf{r}_c-\mathbf{r}_0)}{2(t_c-t_0)}+\frac{(\mathbf{r}-\mathbf{r}_c)\vec{m}(\mathbf{r}-\mathbf{r}_c)}{2(t-t_c)}. \tag{A1}$$

We can solve the problem by minimizing the action, taking the derivative of Eq. (A1) along the surface. Introducing unitary vector $\mathbf{n}$ normal to the surface at the point of collision, we can express the minimization condition as

$$\mathbf{n}\times\nabla_{\mathbf{r}_c}S=0. \tag{A2}$$

Denoting the initial and final velocities as $\mathbf{v}_i=(\mathbf{r}_c-\mathbf{r}_0)/(t_c-t_0)$ and $\mathbf{v}_f=(\mathbf{r}-\mathbf{r}_c)/(t-t_c)$, we can write

$$\mathbf{n}\times\vec{m}(\mathbf{v}_i-\mathbf{v}_f)=0. \tag{A3}$$

This, along with the conservation of energy $E=\mathbf{v}\vec{m}\mathbf{v}/2$, results in Eqs. (3.13). The same result is obtained in the case of stretched boundaries.

APPENDIX B: NUMERICAL METHOD TO SIMULATE THE QUANTUM DYNAMICS

In order to compute the quantum dynamics of the system we resort to a lattice discretization (tight-binding model) in a scale a much smaller than the wavelength of the packets. This condition is relevant to accurately recover the dispersion relation of the free particle $E_k=\hbar^2k^2/(2m)$, from the energy spectrum of the (open boundaries) discretized system,

$$E_k=\frac{2\hbar^2}{ma^2}-\frac{\hbar^2}{ma^2}[\cos(k_xa)+\cos(k_ya)]. \tag{B1}$$

Setting the lattice step as the unit length ($a=1$) we typically worked with $R=20$, except for the calculations in Sec. IV B where, in order to keep the precision for smaller wavelengths, a was reduced keeping the product ka constant.

The discretization results in a Hamiltonian matrix whose diagonal elements are the on-site energies. The off-diagonal elements are hopping terms $V=\hbar^2/(2ma^2)$ which is the maximum kinetic energy represented by the discretization.

The quantum dynamics on the lattice was carried out using a Trotter-Suzuki algorithm,[71] which is a remarkably precise and efficient numerical method. At the lowest order, it is a decomposition of the evolution operator U for a small time τ in a product of analytically solvable evolution operators. Typically one searches for a way to write the Hamiltonian of the system as $\mathcal{H}=\Sigma_k^Q\mathcal{H}_k$, where $\mathcal{H}_k$ are 2×2 matrices, and thus

$$U(\tau)=\exp[i\mathcal{H}\tau/\hbar]\simeq\tilde{U}(\tau)=\prod_k^Q\exp[i\mathcal{H}_k\tau/\hbar], \tag{B2}$$

where $U_k(\tau)=\exp[i\mathcal{H}_k\tau/\hbar]$ are rotation matrices.

The highest orders involve a fractal decomposition of τ that preserves the unitarity of the approximated evolution operator. In our calculations, a fourth-order algorithm with a time step $\tau=0.1\hbar/V$ was precise enough for the time regime of interest.

[1] R. Schuster *et al.*, Nature (London) **385**, 417 (1997).
[2] C.H. Bennet and D.P. DiVincenzo, Nature (London) **404**, 247 (2000).
[3] E.L. Hahn, Phys. Rev. **80**, 580 (1950); R.G. Brewer and E.L. Hahn, Sci. Am. **251** (6), 50 (1984).
[4] W.K. Rhim, A. Pines, and J.S. Waugh, Phys. Rev. Lett. **25**, 218 (1970).
[5] S. Zhang, B.H. Meier, and R.R. Ernst, Phys. Rev. Lett. **69**, 2149 (1992).
[6] P.R. Levstein, G. Usaj, and H.M. Pastawski, J. Chem. Phys. **108**, 2718 (1998).
[7] G. Usaj, H.M. Pastawski, and P.R. Levstein, Mol. Phys. **95**, 1229 (1998); H. M. Pastawski, G. Usaj, and P.R. Levstein, in *Contemporary Problems of Condensed Matter Physics*, edited by S. J. Vlaev, L. M. Gaggero Sager, and V.V. Dvoeglazov (NOVA Scientific, New York, 2001).
[8] H.M. Pastawski, P.R. Levstein, G. Usaj, J. Raya, and J. Hirschinger, Physica A **283**, 166 (2000).
[9] J.M. Ziman, *Electrons and Phonons: The Theory of Transport Phenomena in Solids* (Clarendon Press, Oxford, 1962).
[10] R.B. Laughlin, Nucl. Phys. B (Proc. Suppl.) **3**, 213 (1987).
[11] G. Casati, B.V. Chirikov, I. Guarneri, and D.L. Shepelyansky, Phys. Rev. Lett. **56**, 2437 (1986); F.M. Izrailev, Phys. Rep. **196**, 299 (1990).
[12] F. Haake, *Quantum Signatures of Chaos* (Springer-Verlag, Berlin, 1991).
[13] O. Bohigas, M.J. Giannoni, and C. Schmit, Phys. Rev. Lett. **52**, 1 (1984).
[14] E.J. Heller, Phys. Rev. Lett. **53**, 1515 (1984).
[15] A. Szafer and B.L. Altshuler, Phys. Rev. Lett. **70**, 587 (1993).
[16] A. Peres, Phys. Rev. A **30**, 1610 (1984); in *Quantum Chaos*, edited by H. Cerdeira, R. Ramaswamy, M. C. Gutzwiller, and G. Casati, (World Scientific, Singapore, 1991).
[17] M.A. Nielsen and I.L. Chuang, *Quantum Computation and Quantum Information* (Cambridge University Press, Cambridge, New York, 2000).
[18] R.A. Jalabert and H.M. Pastawski, Phys. Rev. Lett. **86**, 2490 (2001).
[19] W.H. Zurek and J.P. Paz, Phys. Rev. Lett. **72**, 2508 (1994).
[20] F.M. Cucchietti, H.M. Pastawski, and R. Jalabert, Physica A **283**, 285 (2000).
[21] F.M. Cucchietti, H.M. Pastawski, and D.A. Wisniacki, Phys. Rev. E **65**, 045206(R) (2002).
[22] Ph. Jacquod, P.G. Silvestrov, and C.W.J. Beenakker, Phys. Rev. E **64**, 055203 (2001).
[23] W. Wang and B. Li, Phys. Rev. E **66**, 056208 (2002).
[24] D.A. Wisniacki, E.G. Vergini, H.M. Pastawski, and F.M. Cucchietti, Phys. Rev. E **65**, 055206(R) (2002).
[25] F.M. Cucchietti, C.H. Lewenkopf, E.R. Mucciolo, H.M. Pastawski, and R.O. Vallejos, Phys. Rev. E **65**, 046209(R) (2002).
[26] G. Benenti and G. Casati, Phys. Rev. E **65**, 066205 (2002).
[27] N.R. Cerruti and S. Tomsovic, Phys. Rev. Lett. **88**, 054103 (2002); J. Phys. A **36**, 3451 (2003); see also Ref. 30.
[28] T. Prosen, Phys. Rev. E **65**, 036208 (2002).
[29] T. Prosen and M. Znidaric, J. Phys. A **35**, 1455 (2002); T. Prosen, T.H. Seligman, and M. Znidaric, Prog. Theor. Phys. Suppl. **150**, 200 (2003).
[30] N.R.. Cerruti and S. Tomsovic, J. Phys. A **36**, 11 915 (2003); T. Gorin, T. Prosen, and T.H. Seligman, nlin.CD/0311022 (unpublished).
[31] Ph. Jacquod, I. Adagideli, and C.W.J. Beenakker, Europhys. Lett. **61**, 729 (2003).
[32] T. Prosen and M. Znidaric, New J. Phys. **5**, 109 (2003).
[33] B. Eckhardt, J. Phys. A **36**, 371 (2003).
[34] G. Benenti, G. Casati, and G. Veble, Phys. Rev. E **67**, 055202 (2003).

[35] Y. Adamov, I.V. Gornyi, and A.D. Mirlin, Phys. Rev. E **67**, 056217 (2003).
[36] J. Vanicek and E.H. Heller, Phys. Rev. E **68**, 056208 (2003).
[37] G.P. Berman and G.M. Zaslavsky, Physica A **91**, 450 (1978).
[38] W.H. Zurek, Nature (London) **412**, 712 (2001).
[39] Z.P. Karkuszewski, C. Jarzynski, and W.H. Zurek, Phys. Rev. Lett. **89**, 170405 (2002).
[40] D. Weiss *et al.*, Phys. Rev. Lett. **66**, 2790 (1991); **70**, 4118 (1993).
[41] A. Pouydebasque *et al.*, Phys. Rev. B **64**, 245306 (2001).
[42] A. Derode, P. Roux, and M. Fink, Phys. Rev. Lett. **75**, 4206 (1995); A. Kudrolli, V. Kidambi, and S. Sridhar, *ibid.* **75**, 822 (1995); R.A. Méndez-Sánchez, U. Kuhl, M. Barth, C.H. Lewenkopf, and H.-J. Stöckmann, *ibid.* **91**, 174102 (2003).
[43] Ph. Jacquod, I. Adagideli, and C.W.J. Beenakker, Phys. Rev. Lett. **89**, 154103 (2002).
[44] M. C. Gutzwiller, *Chaos in Classical and Quantum Mechanics* (Springer-Verlag, New York, 1990); *Chaos and Quantum Physics*, edited by M.-J. Giannoni, A. Voros, and J. Zinn-Justin, (North-Holland, Amsterdam, 1991).
[45] M. Brack, *Semiclassical Physics*, Frontiers in Physics, Vol. 96 (Westview Press, Boulder, 1997).
[46] K. Richter, D. Ullmo, and R.A. Jalabert, Phys. Rev. B **54**, R5219 (1996); J. Math. Phys. **37**, 5087 (1996).
[47] R.A. Jalabert, in *New Directions in Quantum Chaos*, edited by G. Casati, I. Guarneri, and U. Smilansky (IOS Press, Amsterdam, 2000).
[48] K. Richter, *Semiclassical Theory of Mesoscopic Quantum Systems*, Springer Tracts in Modern Physics Vol. 161 (Springer-Verlag, Berlin, 2000).
[49] As noticed in Ref. 25, the elastic mean free path corresponding to a two-dimensional model of disorder used in Refs. 18,46–48,67, should be affected by a factor of 1/2.
[50] C.F.F. Karney, Physica D **8**, 360 (1983); P. Grassberger and H. Kantz, Phys. Lett. **113A**, 167 (1985).
[51] D.A. Wisniacki and D. Cohen, Phys. Rev. E **66**, 046209 (2002).
[52] V.I. Arnol'd, *Mathematical Methods of Classical Mechanics* (Springer-Verlag, New York, 1978).
[53] J.R. Dorfman, *An Introduction to Chaos in Nonequilibrium Statistical Mechanics* (Cambridge University Press, Cambridge, 1999).
[54] I.L. Aleiner and A.I. Larkin, Phys. Rev. B **54**, 14 423 (1996).
[55] P. Gaspard and G. Nicolis, Phys. Rev. Lett. **65**, 1693 (1990).
[56] H. van Beijeren and J.R. Dorfman, Phys. Rev. Lett. **74**, 4412 (1995); **76**, 3238 (1996).
[57] G. Benettin, L. Galgani, and J.M. Strelcyn, Phys. Rev. A **14**, 2338 (1976).
[58] H.M. Pastawski and G. Usaj, Phys. Rev. B **57**, 5017 (1998).
[59] R. Schack and C.M. Caves, Phys. Rev. E **53**, 3387 (1996).
[60] P.G. Silvestrov, J. Tworzydlo, and C.W.J. Beenakker, Phys. Rev. E **67**, 025204(R) (2003).
[61] H.M. Pastawski, Phys. Rev. B **44**, 6329 (1991); **46**, 4053 (1992).
[62] A.M. Ozorio de Almeida, Phys. Rep. **295**, 265 (1998).
[63] F. Toscano and C.H. Lewenkopf, Phys. Rev. E **65**, 036201 (2002).
[64] U. Weiss, *Quantum Dissipative Systems* (World-Scientific, Singapore, 1993).
[65] W.H. Zurek, Phys. Today **44** (10), 36 (1991).
[66] W.H. Zurek, Rev. Mod. Phys. **75**, 715 (2003).
[67] R.A. Jalabert and H.M. Pastawski, in *Advance in Solid State Physics*, edited by B. Kramer (Springer, Berlin, 2001), p. 41.
[68] D. Monteoliva and J.-P. Paz, Phys. Rev. Lett. **85**, 3373 (2001).
[69] F.M. Cucchietti, D.A.R. Dalvit, J.-P. Paz, and W.H. Zurek, Phys. Rev. Lett. **91**, 210403 (2003).
[70] A. Goussev and J.R. Dorfman, nlin.CD/0307025 (unpublished).
[71] H. De Raedt, Annu. Rev. Comput. Phys. **IV**, 107 (1996).